In: Multiphase Flow Research
Editors: S. Martin and J.R. Williams, pp. 497-542
ISBN: 978-1-60692-448-8

Chapter 9

TWO-PHASE GAS-LIQUID FLOW PROPERTIES IN THE HYDRAULIC JUMP: REVIEW AND PERSPECTIVES

Frédéric Murzyn[1] and Hubert Chanson[2]
[1] ESTACA Campus Ouest, Parc Universitaire de Laval Changé,
Rue Georges Charpak, 53061 Laval Cedex 9, France
[2] Department of Civil Engineering, The University of Queensland,
QLD 4072, Brisbane Australia

Abstract

Research on multiphase flows has been strongly improved over the last decades. Because of their large fields of interests and applications for chemical, hydraulic, coastal and environmental engineers and researchers, these flows have been strongly investigated. Although they are some promising and powerful numerical models and new computing tools, computations can not always solve all actual practical problems (weather forecast, wave breaking on sandy beach...). The recent and significant developments of experimental techniques such as Particle Imagery Velocimetry (PIV) and conductivity or optical probes have particularly led scientists to physical modeling that provide series of data used to calibrate numerical models. Flows with time and length scales that were not achievable in the past are now studied leading to a better description of physical mechanisms involved in mixing, diffusion and turbulence. Nevertheless, turbulence is still not well understood, particularly in two-phase flows.

In the present chapter, we focus on a classical multiphase flow, the hydraulic jump. It occurs in bedrock rivers, downstream of spillways, weirs and dams, and in industrial plants. It characterizes the transition from a supercritical open-channel flow (low-depth and high velocity) to a subcritical motion (deep flow and low velocities). Experimentally, this two-phase flow can be easily studied. Furthermore, it involves fundamental physical processes such as air/water mixing and the interaction between turbulence and free surface. This flow contributes to some dissipation of the flow kinetic energy downstream of the impingement point, in a relatively short distance making it useful to minimize flood damages. It is also associated with an increase of turbulence levels and the development of large eddies with implications in terms of scour, erosion and sediment transport. These are some of the reasons that make studies on this flow particularly relevant. Although numerical and analytical studies

exist, experimental investigations are still considered as the best way to improve our knowledge.

After a brief description of the hydraulic jumps, the first part of this chapter aims to review some historical developments with special regards to the experimental techniques and physical modeling (similitude). In the second part, we describe and discuss the basic properties of the two-phase flow including void fraction, bubble frequency, bubble velocity and bubble size. The free surface and turbulence properties are presented as well. In the last part, we develop some conclusions, perspectives and further measurements that should be undertaken in the future.

Keywords: Hydraulic jump, Two phase flows, Turbulence, Turbulence length and time scales, Froude number, Reynolds number, Void fraction, Free-surface, Bubble frequency

Notations

C	Void fraction defined as the volume of air per unit volume of mixture
C_{max}	Maximum void fraction in the air bubble diffusion layer
D_t	Turbulent diffusivity (m^2/s) of air bubbles in air-water flow
D^*	Dimensionless turbulent diffusivity: $D^* = \frac{D_t}{U_1 d_1}$
d_{mbcl}	Mean bubble chord length (m)
d_1	Upstream flow depth (m)
d_2	Downstream flow depth (m)
F	Bubble count rate (Hz) or bubble frequency
F_{max}	Maximum bubble count rate (Hz) at a given cross-section
Fr	Upstream Froude number
F_{scan}	Sampling rate (Hz)
g	Acceleration of gravity: $g=9.80 m/s^2$
h_c	Channel height (m)
L_c	Channel length (m)
L_f	Longitudinal length scale of turbulence (m) for free surface [42]
L_g	Transversal length scale of turbulence (m) for free surface [42]
L_r	Length of the roller (m)
L_{xx}	Auto-correlation length scale (m) in the bubbly flow [12, 13]
L_{xz}	Transverse air-water integral length scale (m) in the bubbly flow [12, 13]
l_c	Channel width (m)
N_{ab}	Number of air bubbles per record
Q	Water discharge (m^3/s)
Re	Reynolds number: $Re = \frac{\rho U_1 d_1}{\mu} = \frac{U_1 d_1}{\upsilon}$
R_{xx}	Normalized auto-correlation function (reference probe)
R_{xz}	Normalised cross-correlation function between two probe output signals
St	Strouhal number: $St = \frac{F_{toe} d_1}{U_1}$

T	Average air-water interfacial travel time between the two probe sensors (s)
T_{scan}	Sampling duration (s)
T_t	Free surface integral time scale of turbulence measured by wire gages (s)
Tu	Measure of the turbulence level in the air-water flow
T_{xx}	Auto-correlationintegral time scale (s): $T_{xx} = \int_{\tau=0}^{\tau=\tau(R_{xx}=0)} R_{xx} d\tau$
$T_{0.5}$	Characteristic time lag τ for which $R_{xx} = 0.5$ (s)
U_1	Depth-averaged flow velocity upstream of the hydraulic jump (m/s)
x	Longitudinal distance from the upstream gate (m)
x_1	Longitudinal distance from the gate to the jump toe (m)
y	Distance measured normal to the bed channel (m)
y^*	Distance measured normal to the channel bed corresponding to the boundary between the turbulent shear layer and the mixing layer (m)
y_{Cmax}	Distance normal to the bed corresponding to $C=C_{max}$ (m)
y_{Fmax}	Distance normal to the bed corresponding to $F=F_{max}$ (m)
z	Transverse distance from the channel centreline (m)

Greek Symbols

δ	Boundary layer thickness (m)
Δx	Longitudinal distance between probe sensors for dual-tip conductivity probe (m)
ΔH	Head loss (m)
η	Free surface mean level of the jump above the channel bottom (m)
η'	Root mean square of the free surface level fluctuation (m)
ν	Kinematic viscosity of water (m^2/s)
μ	Dynamic viscosity of water (Pas)
ρ	Density of water (kg/m^3)
σ	Surface tension between air and water (N/m)
τ	Time lag (s)
$\tau_{0.5}$	Characteristic time lag for which $R_{xz} = 0.5\ (R_{xz})_{max}$

Subscripts

1	Upstream flow conditions
2	Downstream flow conditions

Abbreviations

PD	Partially-Developed inflow conditions
FD	Fully-Developed inflow conditions

1. Introduction

1.1. Multiphase Flows and the Hydraulic Jump

Multiphase flows are everywhere around us. According to Andrea Prosperetti and Gretar Tryggvason [43], "*it is estimated that over half of anything which is produced in a modern industrial society depends to some extent on a multiphase flow process*". By multiphase flows, we consider a mix of at least two phases among liquid, gas and solid.

In the environment, mixing of air, water and solid particles (sediment) is particularly encountered in coastal and hydraulic engineering. For instance, when a wave breaks on a beach due to a progressive or abrupt modification of the bottom slope, air is entrapped and sediment may also be swept into the water column leading to a complex mix. Figure 1 shows a wave breaking (plunging breaking) on a beach at North Stradbroke Island (Queensland, Australia). The white upper part of the wave is explained by the large amount of air entrapped by the breaking. Scars and turbulent structures are also clearly shown at the free surface on the lower part of this figure that enhance beach erosion or accretion.

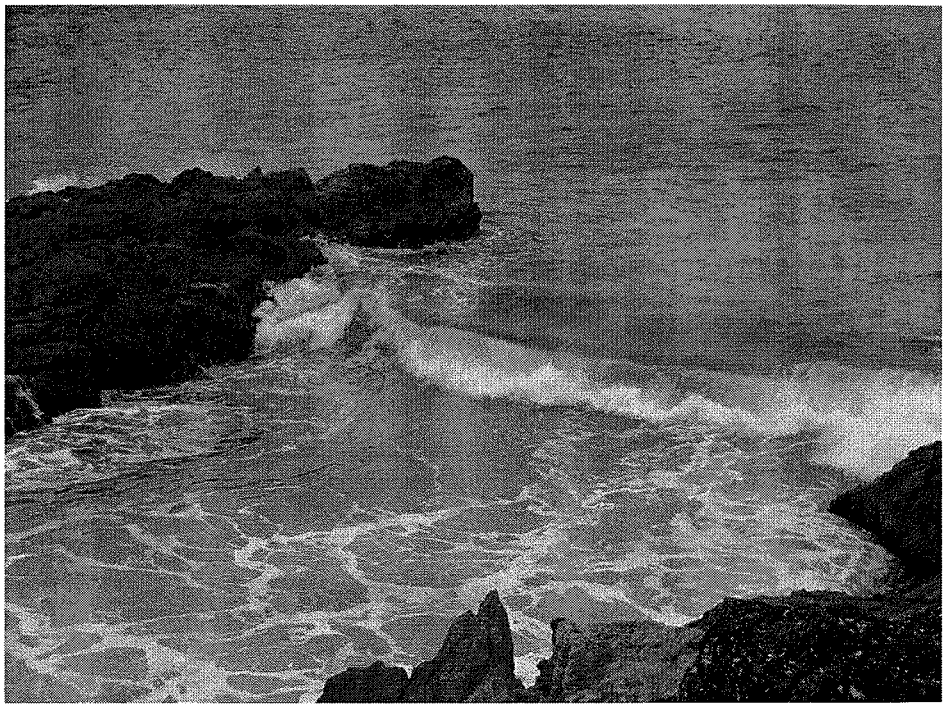

Figure 1. Wave breaking at North Stradbroke Island, Queensland, Australia, June 2007. Photo by Frédéric Murzyn.

In chemical engineering, multiphase flows are involved in flocculation processes with applications to water treatment. The study of chemical mixing is also of primary interest regarding reactor efficiency and diffusion processes. Pollutant transport and dispersion in river streams are among the environmental problems that are linked to multiphase flows as well. In automotive engineering, the mixing of air and fuel (internal combustion engine) is

also of primary importance to improve engine power and reduce pollution with ecological issues. Foam is a substance that is formed by trapping gas bubbles in a liquid. Their low density makes them particularly suitable for thermal insulation, for flotation devices or packing materials. They can also be used as fire retardant when liquid. Multiphase flows are also implied in clouds and rain formation or in pipelines flows.

These examples demonstrate our need to improve knowledge on the topic. Furthermore, these flows imply a wide range of spatial and temporal scales from the millimetric (foams) to geophysical world (cyclone and tropical storms) that require several experimental techniques from the Pitot tube to optical sensors.

In the present chapter, our interest is focused on a classical two-phase flow encountered by coastal and hydraulic engineers: the hydraulic jump. When a transition occurs from a supercritical flow (shallow water, high velocity) to a subcritical motion (deep flow, low velocity), a hydraulic jump takes place. Figure 2 presents the typical sketch of a hydraulic jump. Figure 3 shows a hydraulic jump during a laboratory experiments while Figure 4 shows a hydraulic jumps in nature.

In most laboratory experiments, the hydraulic jump is formed a short distance downstream of the sluice gate ($x_1 < 0.5$ m, Figure 2) and far upstream from a weir located at the end of the channel. Good controls on the flow rate, weir height and aperture beneath the sluice gate ensure the stability of the toe (limited horizontal oscillations, low Strouhal number) and govern the flow regime. Several minutes are generally allowed to elapse before any measurements to ensure good conditions and avoid unexpected effects. The experimental arrangements may sometimes differ.

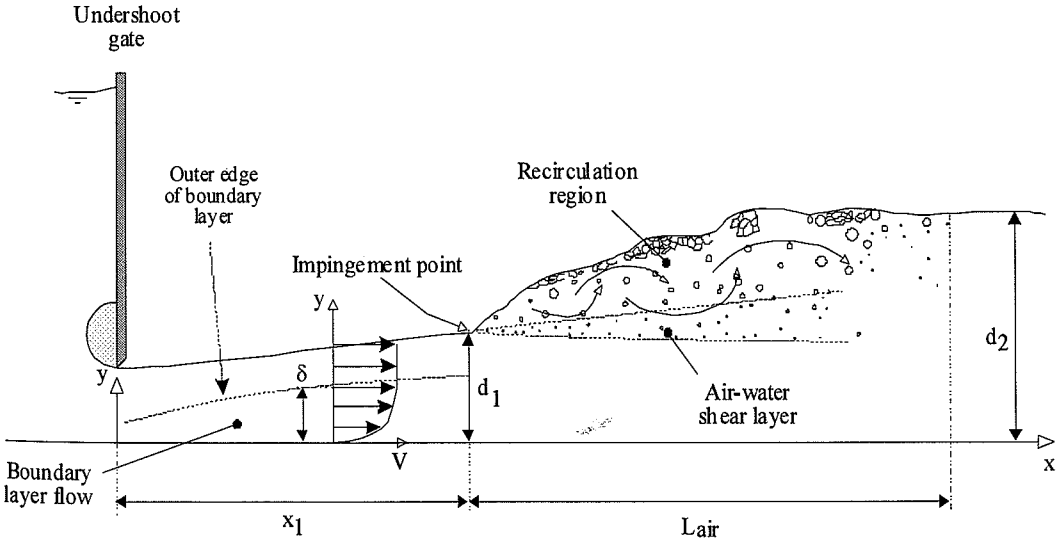

Figure 2. Sketch of a hydraulic jump with relevant notations.

Indeed, an obstacle can be set on the bottom of the channel instead of a sluice gate. The flow section is reduced and the hydraulic jump appears a short distance downstream of the top of obstacle.

Figure 3. Hydraulic jump during laboratory experiments at the University of Southampton (School of Engineering and the Environment, Southampton, UK), Flow from left to right, Fr = 3.65, d_1 = 0.032 m. Photo by Frédéric Murzyn.

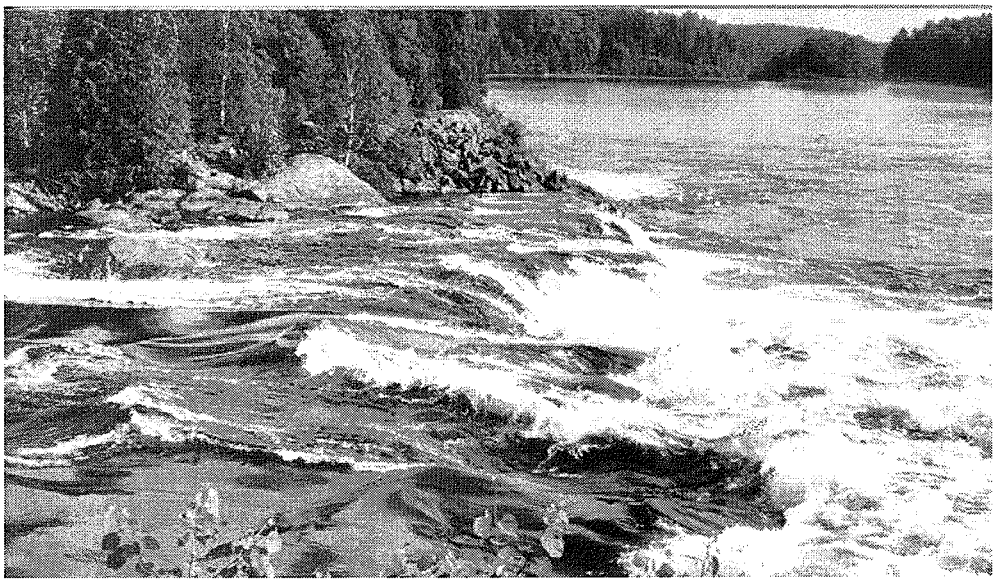

Figure 4. Hydraulic jumps in natural streams in Québec, Canada (Vallée de la Gatineau, Le grand remous, viewed from the right bank, july 2002). Courtesy of Mr and Mrs Chanson.

The hydraulic jump is characterized by a highly turbulent flow with an air-water shear layer and a recirculating area (Figure 2). Macro-scale vortices develop inside and interact with the free surface leading to splashes and droplets formation in the two-phase flow region.

Beyond the region of turbulence production (downstream of the impingement point), some significant kinetic energy dissipation takes place. In terms of environmental aspects, this property is used, for instance, with low impact structures for river restoration and to minimize flood damages.

The main parameter which characterizes the hydraulic jumps is its Froude number defined as:

$$Fr = \frac{U_1}{\sqrt{gd_1}} \tag{1}$$

where U_1 is the inflow velocity (m/s), d_1 is the inflow water depth (m) and g is the acceleration of gravity (m/s^2).

The Froude number is always greater than 1 for hydraulic jumps. Depending on that dimensionless number, different kinds of jumps are referenced including [7, 10, 15, 16]:

- The undular hydraulic jump for $1 < Fr < 1.5$ to 4;
- The breaking jump for larger Froude numbers encompassing the oscillating jump studied by Mossa [35] and the steady jump for large Froude numbers.

The study of Gualtieri and Chanson [28] showed that the air-water flow properties were similar in both steady and strong jump flows.

For a horizontal rectangular channel and neglecting boundary friction, the continuity equation leads to Bélanger equation [2, 6, 7, 15]:

$$\frac{d_2}{d_1} = \frac{1}{2}\left(\sqrt{1+8Fr^2} - 1\right) \tag{2}$$

where d_1 is the inflow water depth (m) at the impingement point and d_2 is the downstream flow depth (m) far from the impingement point.

The hydraulic jump is mainly used as an energy dissipator [6, 7, 10, 29]. The stronger the jump is, the highest the energy dissipation is. The dimensionless head loss is given by:

$$\frac{\Delta H}{d_1} = \frac{\left(\sqrt{1+8Fr^2} - 3\right)^3}{16\left(\sqrt{1+8Fr^2} - 1\right)} \tag{3}$$

For steady hydraulic jump, the energy dissipation goes from 45% to 70%. It reaches up to 85% for strongly turbulent jump. Although hydraulic jumps dissipate a large part of the incoming flow energy, the high levels of turbulence in these flows tend to increase scour and erosion at bridge piers or in rivers (Figures 5 and 6).

For physical modeling and similitude purposes, the Reynold number (Re) is often used as well to characterize the flow:

$$Re = \frac{U_1 d_1}{\upsilon} \tag{4}$$

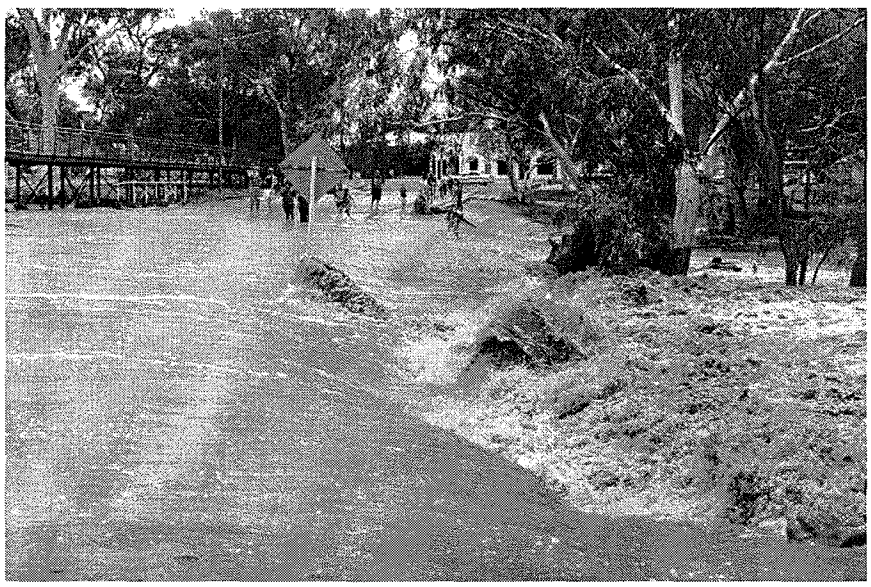

Figure 5. A large flood flow of the Todd river in Alice Springs (NT, Australia), January 2007. Flow from left to right. Courtesy of Sue McMinn.

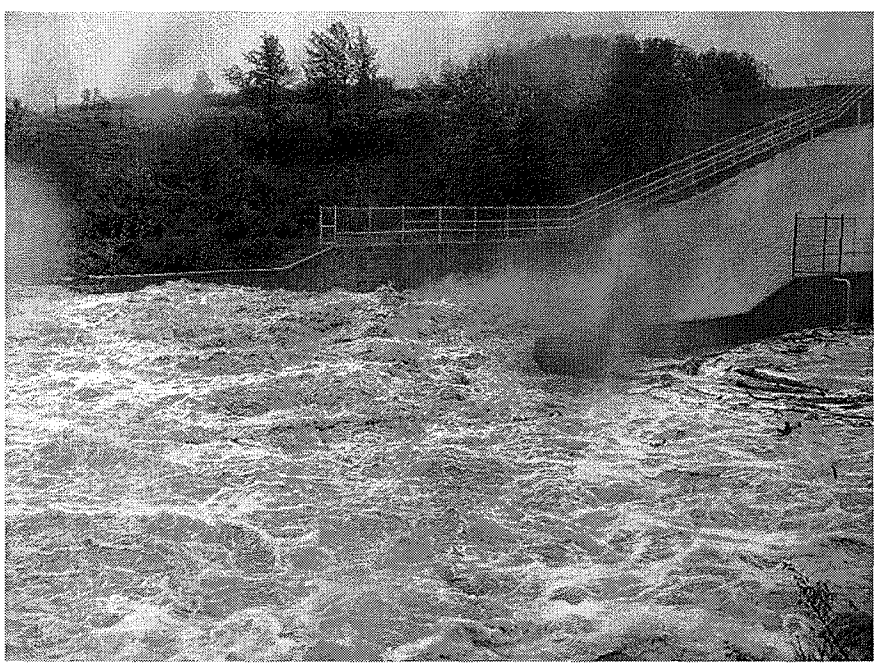

Figure 6. Hydraulic jump stilling basin and spillway on Chain Lakes dam (Southern Alberta, Canada), June 2005. Flow from top right to bottom left. Courtesy of John Remi.

Figure 7. River kayaking at Flage (Norway). Courtesy of Øyvind Thiem.

On Figure 5, the current strength is clearly seen by looking at the foot of the road panel. Here, the formation of the hydraulic jump is caused by the sudden and abrupt change on the road profile. Note the brown color of the water which carries solid particles.

On Figure 6, the upcoming supercritical flow (right top of the picture) becomes subcritical (lower part). At the bottom of the spillway, a transition occurs leading to a turbulent shear flow with macro-vortices associated with large and rapid fluctuations of the free surface, strong mixing and scars that both enhance mixing and energy dissipation. Note that droplets and splashes can be observed on this figure.

When the weather conditions are "good", hydraulic jumps are also much appreciated by kayakers and surfers. They become funny spots as illustrated by Figures 7 and 8.

After strong rains, the flow rate of some rivers strongly increases. Particularly in mountain areas, the river beds are generally made of gravels with strong and sudden flow depth variations. Hydraulic jumps are not rare providing some wonderful spots for funny moments.

On Figure 8, a spilling breaker is ridden by a surfer while a second surfer is waiting for the next wave. This picture illustrates once again the strong interest of researchers and engineers for the hydraulic jump: the hydraulic jump may be considered as a steady spilling breaker. As a consequence, the broad spectrum of situations where hydraulic jumps take place has reinforced our need to explore this exciting two-phase flow. Air/water mixing, bubble dynamics, sediment transport, erosion and scour, bubble coalescence, free surface and turbulence interactions and wave breaking processes are among research topics that can be studied through hydraulic jumps.

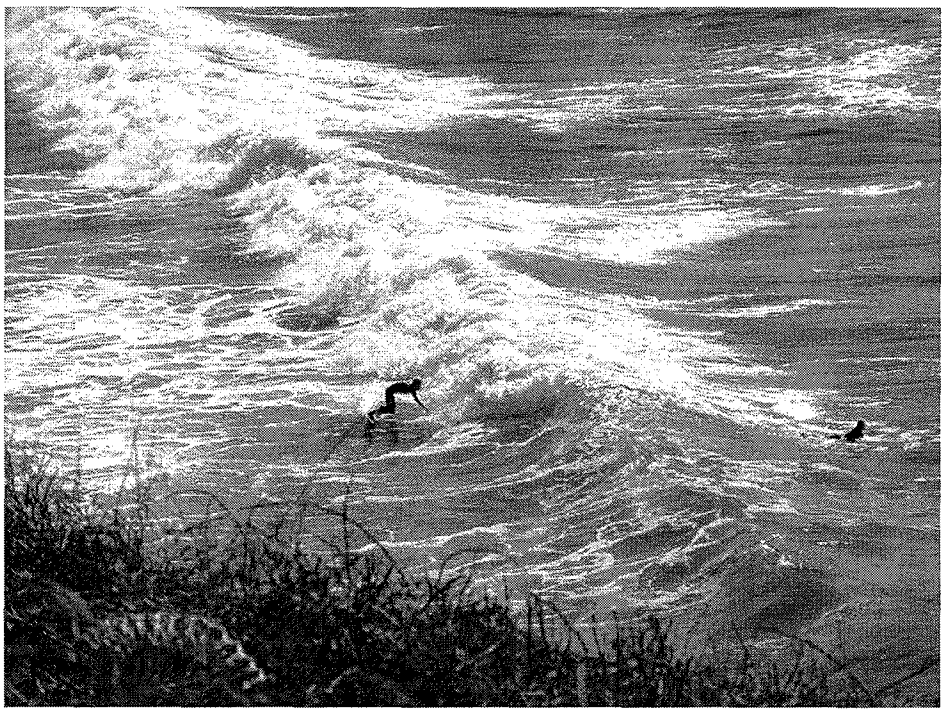

Figure 8. Surfers and spilling breaker on Plage du Minou. Viewed from Pointe du Grand Minou (Hameau de Toulbroc'h), March 2004 (Mid flood tide). Photo by Hubert Chanson.

1.2. Reviews of Historical Works and Experimental Techniques

In this part, we aim to review some of the most significant contributions on hydraulic jumps. In the last 50 years, many studies have been undertaken through numerical, analytical and experimental (physical) modeling requiring a wide range of instrumentation. Table 1 summarizes the main experimental studies that have been undertaken on hydraulic jumps in the last 50 years. This review is not exhaustive but encompasses the some significant contributions obtained with different experimental techniques over the last 50 years. Here, we are particularly interested in experimental contributions. Indeed, although some recent developments, numerical and analytical approaches are not yet enough accurate or developed to give exact solutions. The complexity of the flow and the high number of equations to solve make such computations too difficult.

The first significant experimental contributions have been made by Rajaratnam [44, 45]. In 1965, he gave a description of the velocity fields in hydraulic jumps using a Pitot-Prandtl tube [45]. He particularly showed the analogy between the wall-jet flow and non-aerated hydraulic jumps. Indeed, he observed the development of a boundary layer next to the bed characterized by a rapid increase of the velocity over a thin layer above the channel bottom. Then, a gradual decrease was measured. These results followed a first extensive study made by Rajaratnam in 1962 where conductivity probes were used to present some basics results on bubbly flow properties such as the void fraction [44].

Ten years later, Resch and Leutheusser [46, 47] have probably brought one of the most important contribution (to date) on the topic. Their results were obtained with conical hot-film

probes in the bubbly flow region. Resch and Leutheusser have mainly showed that the air entrainment, momentum transfer and energy dissipation processes were strongly affected by the incoming flow conditions. This point is fundamental and means that the quality of the results depends on the experimental conditions. As a consequence, the relative boundary layer thickness (δ/d_1) developing upstream of the impingement point is a key-point that affect the bubbly flow. Depending on this relative boundary layer thickness, the inflow conditions are either partially developed (PD) or fully developed (FD) (Table 1). Murzyn et al. [41] gave an estimation of their boundary layer thickness developing over a flat bed made of PVC. They found that $0.18d_1 < \delta < 0.36d_1$ which corresponds to partially-developed (PD) inflow conditions.

In 1981, Babb and Aus [1] used conical hot film probes which sizes were smaller than those of Resch and Leutheusser. This point is of interest. Indeed, intrusive probes may disturb the flow. In hydraulic jumps, this is particularly true in the upper part of the flow where negative horizontal velocities are observed. Thus, the disturbances caused by the probes propagate upstream leading to some possible significant flow modifications. Thus, intrusive probes must be as small as possible to minimize such disturbances and optimize the accuracy of the results. Babb and Aus investigated the movement of air bubbles in and out of the jump for one experimental condition (Fr = 6). They found that large bubbles were mostly located near the impingement point. Their lifetime was very short because of the turbulence, shear and buoyancy.

In the last years, the improvement of these experimental techniques in terms of response times, spatial and temporal resolution or data analysis procedures has led to an extraordinary number of studies with either conductivity and optical probes, wire gages or flow visualizations [5, 11, 12, 13, 14, 15, 16, 19, 23, 28, 31, 32, 33, 35, 36, 37, 38, 39, 40, 41, 42, 48].

Since the beginning of the 90's, the most important contributions are probably those of Chanson [5, 11, 12, 13, 14, 15, 16], Chanson and Brattberg [19], Gualtieri and Chanson [28], Mossa [35, 36], Kucukali and Chanson [31], Mouazé et al. [37] or Murzyn et al. [41, 42]. Other contributions include [23, 31, 38, 39, 40]. They have brought new developments leading to a better understanding of the physical mechanisms involved in hydraulic jumps. Nevertheless, this is not enough.

Chanson [5], Chanson and Brattberg [19], Chanson and Toombes [24] have preferentially used conductivity probes (single or dual tip conductivity probes) which have been manufactured, tested and used at the University of Queensland with a range of sensor size from 0.025 mm to 0.35 mm including 0.1 mm and 0.25 mm. These phase-detection probes are designed to pierce bubbles. Based upon the difference of electrical resistivity between air and water, they are well-adapted for bubbly flows such as hydraulic jumps. Figure 9 presents a sketch of a single-tip probe. For instance, the study of Chanson and Brattberg [18] used a 0.025 mm sensor size.

When the sensitive part of the probe is in water, current flows between the tip and the supporting metal. Then, an output voltage is collected. It becomes nearly null when the tip is in air. Because the output voltage is subject to some fluctuations caused by dust flowing in water, a single threshold technique is applied on the output signal to define time lags corresponding to air and water [31, 38].

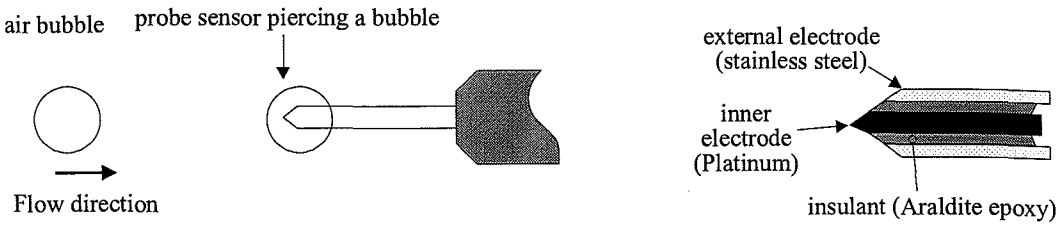

Figure 9. Sketch of the single-tip conductivity probe (Left: bubble piercing, Right: sketch of the tip).

Data analysis on this voltage provides basic information on the bubbly flow such as the void fraction (C), the bubble frequency (F) and bubble size (d_{mbcl}).

The main strength of these intrusive sensors concerns their size (0.35 mm or 0.25 mm). Thus, they are enough accurate to detect very small bubbles (down to the size of the sensor). Their dynamic response time is high (less than 10μs). This makes them accurate and suitable for measurements in highly turbulent and fluctuating flows such as hydraulic jumps.

Chanson [5, 12] first detailed the air-water mixing processes providing pertinent information on void fraction, bubble frequency, bubble size and bubble velocity downstream of the impingement point. His main conclusions concern:

- The void fraction (C): in the turbulent shear layer, C satisfies a diffusion equation. Then, the vertical profiles of C fit a gaussian distribution given by:

$$C = C_{max} \exp\left(-\frac{\left(\frac{y - y_{C_{max}}}{d_1}\right)^2}{4D^*\left(\frac{x - x_1}{d_1}\right)}\right) \quad (5)$$

- The bubble frequency (F): in the bubbly flow region, the vertical profiles of F exhibit two distinctive peaks. The major peak is found to be in the turbulent shear layer while the second minor peak is mostly found in the mixing layer ;
- The vertical positions of the maximum of void fraction (y_{Cmax}/d_1) and bubble frequency (y_{Fmax}/d_1): they do not coincide showing two competitive diffusion processes ;
- The importance of scale effects: the dynamic similarity (Froude similitude) is important and some scale effects may arise for largest Reynolds numbers ($Re > 10^5$).

When a dual-tip conductivity probe is used (Figure 10), further information can be obtained such as the bubble velocity (V), turbulence levels (Tu) which correspond to the fluctuations of the air-water interfacial velocity and some time (T_{xx}) and length (L_{xx}, L_{xz}) scales of turbulence [12, 13] representing the turbulent structures of the flow. New results have been discussed by Kucukali and Chanson [31] and Murzyn and Chanson [38, 39, 40]. The turbulence length and time scales bring new information on the physical mechanisms involved in such flows that may be useful to calibrate numerical models (mesh size, spatial and temporal resolutions...). They will be discussed in the present chapter.

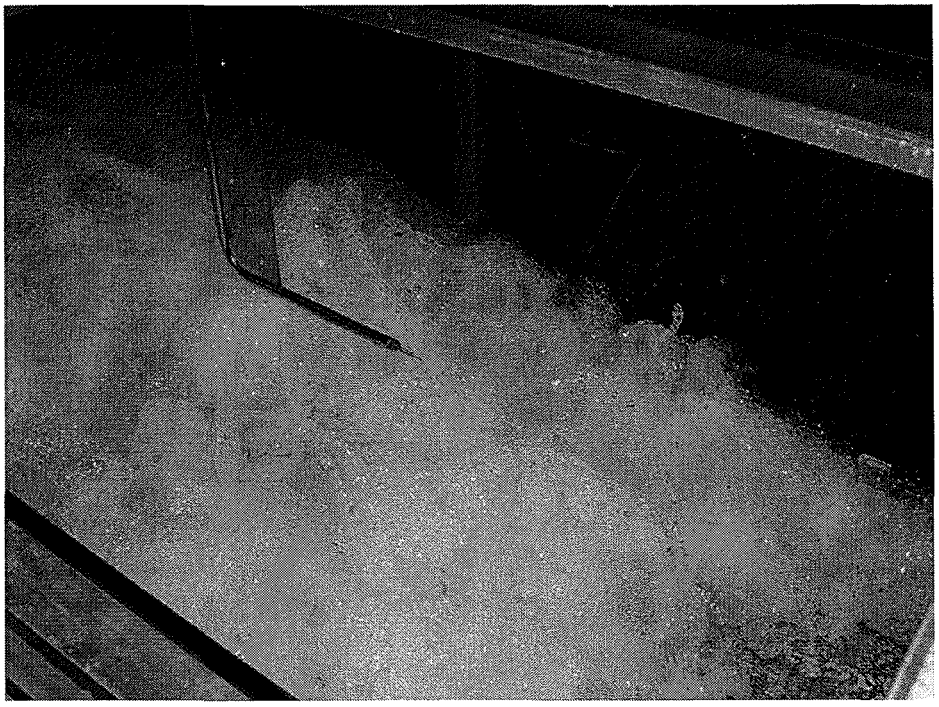

Figure 10. Dual-tip conductivity probe at the University of Queensland. The inner electrode diameter is 0.25 mm and the longitudinal distance between both tips is $\Delta x = 7$ mm. Flow from right to left, $d_1 = 0.018$ m, $x_1 = 0.75$ m, Fr = 8.45, $U_1 = 3.6$ m/s.

Table 1. Most significant experimental investigations of hydraulic jumps

References	Fr	Re	Measurement techniques	Comments
Rajaratnam 1962 [44]	2.68 to 8.72	34000 to 110500	Conductivity probes	1/8 inch diameter copper tube leaving a length of 1/64 inch bare at the bottom and fitted inside a brass tube leaving a conducting ring of 1/64 inch in length at the bottom
Rajaratnam 1965 [45]	2.68 to 9.78	52500 to 128000	Prandtl type Pitot static tube	3 mm external diameter, hemispherical head
Resch and Leutheusser 1972 [46, 47]	2.98 to 8.04	33360 to 71760	Conical hot-film probe	0.6 mm sensor size Partially and Fully-developed inflow conditions
Babb and Aus 1981 [1]	6.00	122850	Conical hot-film probe	0.4 mm sensor size Partially developed inflow conditions

Table 1. Continued

References	Fr	Re	Measurement techniques	Comments
Chanson 1995 [5]	5.10 to 8.60	39500 to 63800	Pitot tube + single and dual-tip conductivity probe	Pitot tube: 3.3 mm external diameter Conductivity probe: single tip (0.35 mm inner electrode) Partially-developed inflow conditions
Mossa and Tolve 1998 [36]	6.42 to 7.30	57300 to 58000	Video camera CCD	CCD 200,000 pixels Partially-developed inflow conditions
Chanson and Brattberg 2000 [19]	6.33 to 8.48	36120 to 48580	Pitot tube + dual-tip conductivity probe	Dual-tip: 25 μm inner electrode Partially-developed inflow conditions
Waniewski et al 2001 [48]	11.5 to 19.3	10940 to 16680	Phase Doppler Anemometry	Resolution: 1μm
Liu et al 2004 [33]	2.00 to 3.32	86100 to 147680	Micro Acoustic Doppler Velocimeter	1 mm diameter conical sapphire tip
Murzyn et al 2005 [41], 2007 [42]	2.00 to 4.80	45990 to 88500	Optical fibre probes (double and single tips) Wire gages	0.010 mm sensor size, 1 mm tip spacing Sampling rate up to 1 MHz Two thin wire: 1 mm apart Partially-developed inflow conditions
Lennon and Hill 2006 [32]	1.40 to 3.00	23930 to 27940	Single camera Particle Image Velocimetry	
Chanson 2006 [5]	5.00 to 8.10	31500 to 51000 *(Estimation)*	Single-tip conductivity probes Pitot tube (3.3 mm external diameter)	Inner electrode: 0.35 mm in diameter Partially-developed inflow conditions
Chanson 2007 [12, 13]	4.60 to 8.60	25000 to 98000	Single-tip conductivity probes	Inner electrode: 0.35 mm in diameter Partially-developed inflow conditions
Gualtieri and Chanson 2008 [28]	5.20 to 14.3	24680 to 58000	Single-tip conductivity probe	Inner electrode: 0.35 mm in diameter Partially-developed inflow conditions

Table 1. Continued

References	Fr	Re	Measurement techniques	Comments
Murzyn and Chanson 2007 [38], 2008 [39, 40]	5.10 to 8.30	38550 to 64100	Dual-tip conductivity probes	0.25 mm inner electrode, 7 mm tip spacing Partially-developed inflow conditions

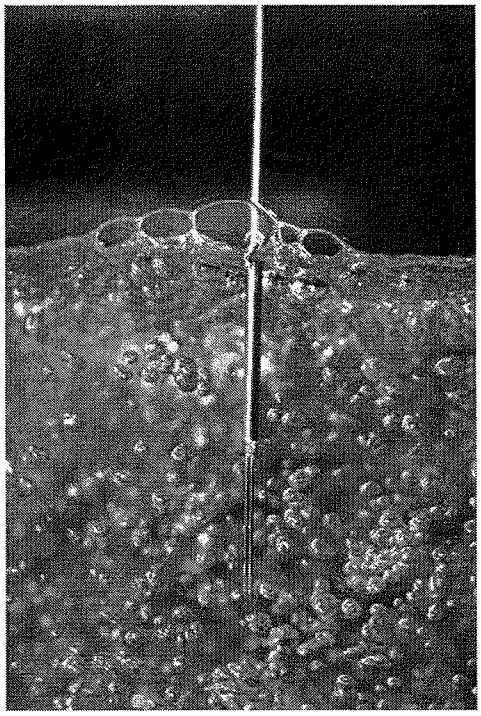

Figure 11. Optical fibre probe in bubbly flow. The presence of air or water is detected at the ends of each two parallel 10 μm diameter optical fibre probes, 1 mm apart and situated in the circle (although non visible). The fibres extend 5 mm beyond the end of 25 mm long, 0.8 mm diameter cylindrical supports. Photo by Frédéric Murzyn.

In 2005, Murzyn et al. [41] published their results on hydraulic jumps obtained with optical fibre probes. This is an intrusive technique in which tips are also designed to pierce bubbles. The difference compared to conductivity probes is that, in this case, the detection of air or water is based upon the difference of the refractive index between both media. This is a robust and highly accurate technique as the sensor tip size is only 0.01 mm (Figure 11). Bubbles size down to 10 μm can thus be detected. Furthermore, the response time of this probe is less than 1μs making the optical probe well-adapted to scan rapidly-changing and highly turbulent two-phase flows. Their results showed that the data were consistent down to $C = 0.001$ or better. This is certainly better than for conductivity probes. In the mixing layer, they also found that all vertical void fraction profile fit an error function whatever the Froude number is. Coupled with the results of Chanson [11], a complete description of the vertical

void fraction profiles is available in the turbulent shear layer as well as on the mixing layer for a wide range of Froude numbers ($2 < Fr < 8.5$).

Murzyn et al. [42] have also investigated the free surface motion using two home-made thin wire gages (diameter = 0.05 mm, 1 mm apart). New description of the free surface dynamics has been made in order to investigate the free surface interaction with turbulence. This part may be considered as independent of the bubbly flow. Nevertheless, the free surface behavior strongly influences the flow dynamics. Thus, it will be discussed in this chapter as well. Concerning the free surface levels, their results pointed out a peak of turbulent fluctuations in the first half of the roller where turbulence production is the most intense. Downstream of this maximum, turbulence levels regularly decreased to reach smallest levels. Furthermore, using a correlation technique, typical length scales have also been estimated to be smaller than $5d_1$ depicting the turbulent structures developing at the free surface and indicating that the upstream conditions have some influence on the predominant scales of the flow. Other contributions were obtained in different ways with different goals. They refer either to non intrusive techniques such as PIV or LDV or to other intrusive techniques that were not fully satisfying.

A relevant contribution has been made by Mossa and Tolve [36]. Using a video camera, they proposed to analyze the air concentration in hydraulic jumps through image processing. Their non invasive technique was able not only able to evaluate air concentration successfully but also to visualize coherent structures of turbulence. Nevertheless, they were limited in terms of experimental conditions. Indeed, only three Froude numbers (in the same range) were studied. Anyway, their technique seemed to be very promising and would need further investigations.

Figure 12. LDV measurements in hydraulic jumps at the University of Caen (France) in 2002. Flow from right to left. The hydraulic jump is formed by a round-shaped obstacle situated on the bottom of the channel. The four Laser beams (two green and two blue) converge at the measurement point. With this 2D system, both horizontal and vertical components of the velocity are simultaneously recorded.

Following the development of new experimental techniques in fluid mechanics such as Laser Induced Fluorescence (LIF) or Particle Tracking Velocimetry (PTV), Laser Doppler Velocimetry (LDV) and Particle Imagery Velocimetry (PIV) have really been important over the ten past years. For instance, figure 12 shows LDV measurements in hydraulic jumps (upstream part of the jump).

PIV systems have been for all kind of applications including in-situ measurements. Theoretically, this is a non intrusive technique although it is now used in natural environments such as seas or oceans. It offers many advantages such as high spatial and temporal resolution and 2D/3D instantaneous measurements of velocity fields.

As a non invasive optical technique (in laboratory experiments), it is particularly well-suited for monophase flows. Indeed, the measurement system consists on a thin Laser sheet lighting a region of the flow. Positions of particles situated in this Laser sheet are recorded. Correlation analysis of these particle positions between different images leads to the corresponding velocity vectors. Actually, this is probably the most powerful technique for flow velocity, vorticity and turbulence measurements in liquid or gas flows. Nevertheless, recent studies have started on two-phase flows and particularly on hydraulic jumps (but limited to low Froude numbers).

Lennon and Hill [32] tended to scan the flow in hydraulic jumps using Particle Imagery Velocimetry (PIV) system. The technique is necessarily quite limited in hydraulic jumps with high Froude number because of the large amount of bubbles that disturb the optical path of the Laser sheet. Thus, their experimental works were limited to Fr = 1.37, 1.65 and 3.0. In the two first cases, the jumps were undular while the last one has a low rate of air entrainment. Nevertheless, they obtained some plots of mean velocities and vorticity. This first approach is interesting but seems to be limited to low-aerated flows. Indeed, they argued that "*the problem with very bubbly flows, however, is that the bubbles distort the optical rays between the image and the acquisition plane. Despite the relatively short optical path in the present experiments, a high bubble fraction will blur the images of the illuminated seed particles resulting in poor image correlations. As such, optical and methods such as PIV and LDV will have the same difficulties as acoustic and thermal methods when it comes to turbulence measurements in a highly aerated roller*".

Liu et al. [33] used a microADV to measure the flow velocity in free hydraulic jumps with Froude numbers of 2.0, 2.5 and 3.32. They found that this acoustic method was not accurate enough due to boundary effects that strongly increase the relative error on velocity measurements. Compared to Prandtl tube, the error on mean velocity measured by the ADV increased linearly with the air concentration at very low void fraction. Matos et al. [34] found that accuracy of ADV is limited in two-phase flows when void fraction exceeds 8 %. Thus, it is reasonable to think that ADV are not well-suited for studies in hydraulic jumps with large Froude numbers.

This review of the most significant experimental contributions on hydraulic jumps leads to different conclusions. Although some new powerful techniques are available for researchers and scientists such as PIV, LDV or ADV, it is still believed that the most accurate techniques are conductivity and optical probes. These intrusive methods have proven their robustness in terms of response time and space-time resolutions. Particularly, they were used by Rajaratnam [44], Chanson [5, 11, 12, 13] and Murzyn et al. [41]. Furthermore, the small size of tips limits weak effects. The Reynolds number associated with the flow past the probe is low. For instance, it was less than 30 in the measurements of Murzyn et al. [41]. This

contributes to minimize uncertainty on measurements. Optical probes can measure bubble sizes down to 10 μm and void fraction down to 0.001 or better.

Concerning the data acquisition, attention must be focused on duration and sampling rate to ensure their quality. For conductivity probes, Chanson [12, 14] performed a sensitivity analysis on the effects of sampling duration T_{scan} and sampling rate F_{scan} on void fraction and bubble count rate in hydraulic jumps. The sampling duration was selected within the range $0.7 \text{ s} < T_{scan} < 300 \text{ s}$ and the sampling rate was between $600 \text{ Hz} < F_{scan} < 80 \text{ kHz}$. First, the data showed that the sampling rate had almost no effect on the void fraction for a given sampling duration. However, the bubble count rate was underestimated for sampling rates below 5 to 8 kHz. Second, the sampling duration had little effect on both void fraction and bubble count rate for scan periods longer than 30 to 40 s. Then, he recommended a sampling duration of 45 s and a sampling rate of 20 kHz. For optical probes, Murzyn et al. [41] acquired their data during a maximum sampling duration of 120 seconds. Nevertheless, as soon as 10000 bubbles were recorded, data acquisition stopped. To date, these experimental conditions are supposed to be large enough.

1.3. Physical Modeling of the Hydraulic Jump

Hydraulic jumps are commonly encountered in natural streams. This complex two-phase flow always requires more and more investigations. Despite numerous studies over the last decades, there is still a lack of knowledge on the physical mechanisms involved in diffusion, turbulence and mixing processes occurring in such flows. Thus, developments of numerical codes, analytical methods and experimental works are fundamental to improve our knowledge on the flow dynamics. Nevertheless, analytical and numerical studies of multiphase flows are quite difficult due to the large amount of relevant equations to solve. Furthermore, many interactions take place between bubbles, droplets, particles, free surface, turbulence that make analytical methods quite limited. The same complexity often imposes reduced descriptions (averaged equations, basic hypothesis) for numerical modeling which can then not be fully successful and satisfying.

Experimental investigations are thus required to help numerical modelers to calibrate their codes with empirical data. This is the strong interaction between numerical and experimental studies that will lead research to a better knowledge of the physical mechanisms involved in these flows. Experimental investigations are numerous and many sets of data are available in the literature regarding the two-phase flow properties (void fraction, bubble frequency, bubble velocity...). These were mainly obtained using phase-detection probes (optical fibre probes or conductivity probes). The accuracy of these measurements, the results and their meanings for natural flows are not only linked to the data acquisition parameters but also to the experimental conditions (similitude). Data interpretation (extrapolation) to natural streams requires some similitude criterion that must be achieved (geometric, kinematic or dynamic similitude). Generally-speaking, two-phase flow laboratory experiments are based on a geometric similitude. This means that model and prototype scales are geometrically similar. Note that dynamic similitude is sometimes used as well.

In fluid mechanics, the governing equations for fluid flow motion are known as the Navier-Stokes equations. In a free surface open-channel flow, gravity effect can not be neglected. The corresponding Navier-Stokes equations are then given by:

$$\begin{aligned}\frac{du}{dt} &= -\frac{1}{\rho}\frac{\partial p}{\partial x} + \upsilon\Delta u \\ \frac{dv}{dt} &= -\frac{1}{\rho}\frac{\partial p}{\partial y} + \upsilon\Delta v \\ \frac{dw}{dt} &= -\frac{1}{\rho}\frac{\partial p}{\partial z} - g + \upsilon\Delta w\end{aligned} \tag{6}$$

Where (u, v, w) are the velocity components (m/s), ρ the density of water (kg/m^3), p the pressure (Pa), g the acceleration of gravity (m/s^2), (x, y, z) the coordinate axis (z positive upward), ν the kinematic viscosity of water (m^2/s).

To date, these nonlinear differential equations remain still unsolved. Indeed, turbulent flows are characterized by random processes that can not be exactly modeled unless some restrictive hypothesis. To date, only approximated solutions can be proposed. That is one of reason which explains why weather forecasts become meaningless after more than 1 week. This is partially due to random and unpredictable phenomena that may occur between forecasts and reality. It is not unbelievable to think that the Navier-Stokes equation will remain unsolved for a long time. This partially explains the limited number of numerical studies on hydraulic jumps compared to experimental investigations: modeling turbulence is difficult but modeling turbulence of two-phase flows becomes nearly impossible.

Equations (6) are not dimensionless. To make them so, let us introduce new dimensionless variables:

$$\begin{aligned}x^+ &= \frac{x}{d_1} \; ; \; y^+ = \frac{y}{d_1} \; ; \; z^+ = \frac{z}{d_1} \\ u^+ &= \frac{u}{U_1} \; ; \; v^+ = \frac{v}{U_1} \; ; \; w^+ = \frac{w}{U_1} \\ t^+ &= \frac{U_1}{d_1}t \; ; \; p^+ = \frac{p}{\rho U_1^{\,2}}\end{aligned} \tag{7}$$

Then, let us introduce them in equations (6). We obtain new dimensionless Navier-Stokes equations given by:

$$\begin{aligned}\frac{du^+}{dt^+} &= -\frac{\partial p^+}{\partial x^+} + \frac{1}{Re}\Delta u^+ \\ \frac{dv^+}{dt^+} &= -\frac{\partial p^+}{\partial y^+} + \frac{1}{Re}\Delta v^+ \\ \frac{dw^+}{dt^+} &= -\frac{\partial p^+}{\partial z^+} - \frac{1}{Fr} + \frac{1}{Re}\Delta w^+\end{aligned} \tag{8}$$

To ensure similarity between model (laboratory) and prototype (at scale), one must ensure that Navier-Stokes equations are similar in both cases. Indeed, same equations will

have same solutions. For a free-surface open-channel flow (such as the hydraulic jump), this is achieved when Froude and Reynolds numbers for model and prototype are equal (Eq. 8). Theoretically, this means that Froude and Reynolds similitude must be simultaneously achieved. Unless rare cases, they can not be simultaneously achieved. Nevertheless, for a free surface flow, the Reynolds condition may be eliminated when diffusion process can be neglected (Re >> 1).

The dimensional analysis proposed by Chanson [12] leads to a similar conclusion. Considering a hydraulic jump in a horizontal, rectangular channel, it is supposed that all flow properties (C, F, U, d_{mbcl},...) depend on the fluid and experimental set-up properties. That is:

$$C, F, U, d_{mbcl}, ... = F_1\left(x, y, z, d_1, \delta, \upsilon_{air}, \upsilon_{water}, \rho_{air}, \rho_{water}, ...\right) \quad (9)$$

where C is the void fraction, F the bubble frequency, V the velocity, d_{mbcl} the mean bubble chord length, x, y and z the coordinates, ν_{air} and ν_{water} the kinematic viscosity of air and water respectively, ρ_{air} and ρ_{water} the density of air and water respectively. δ is the boundary layer thickness of the inflow (defining partially or fully-developed inflow conditions). Neglecting compressibility effects, one can ignore ρ_{air} and ν_{air} such as equation (9) may be expressed in dimensionless terms:

$$C, \frac{F d_1}{V_1}, \frac{U}{\sqrt{g d_1}}, \frac{d_{mbcl}}{d_1}, ... = F_2\left(\frac{x - x_1}{d_1}, \frac{y}{d_1}, \frac{z}{d_1}, \frac{U_1}{\sqrt{g d_1}}, \frac{U_1 d_1}{\upsilon}, ...\right) \quad (10)$$

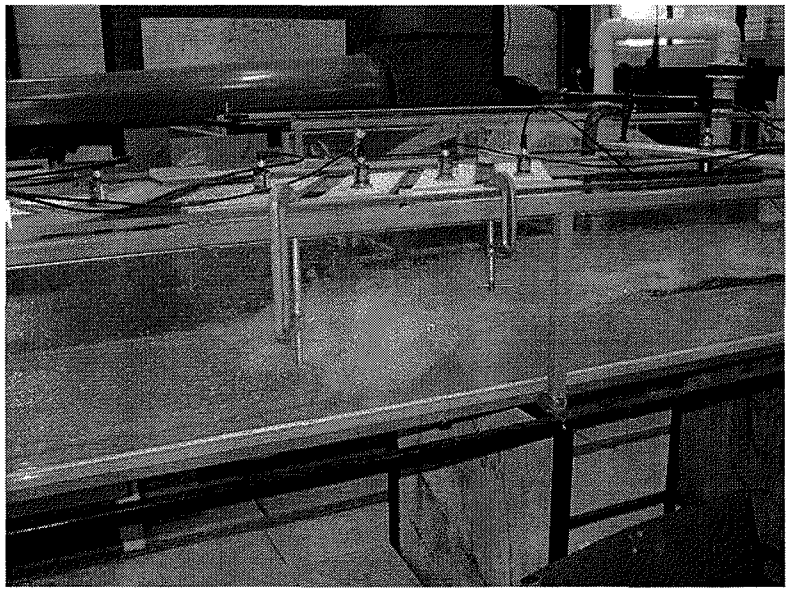

Figure 13. Hydraulic jump at the University of Queensland, flow from left to right, d_1 = 0.018 m, x_1 = 0.75 m, Fr = 5, Re = 37800, U_1 = 2.1 m/s, PD inflow conditions. Photo by Hubert Chanson.

In the right hand side of equation (10), Froude and Reynolds numbers appear in fourth and fifth positions respectively. Chanson [12] found that significant scale effects in terms of

air-water flows properties (void fraction, bubble count rate and bubble chord time distributions) may arise if only a Froude similitude is used. Thus, attention must be drawn on Reynolds number as well. Recently, Gualtieri and Chanson [28] analyzed Froude number effect on air entrainment in the hydraulic jumps with Froude numbers up to 14.3. They showed that aeration properties are enhanced by higher Froude numbers.

Figures 13 and 14 show some laboratory experiments on hydraulic jumps at the University of Queensland. The channel was 3.2 m in length, 0.50 m in width and 0.45 m in height.

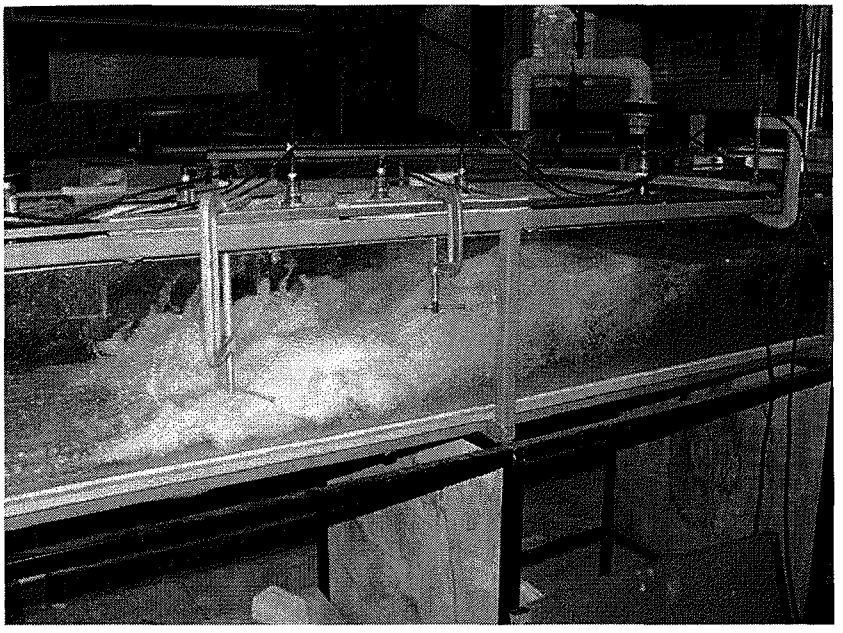

Figure 14. Hydraulic jump at the University of Queensland, flow from left to right, d_1 = 0.018 m, x_1 = 0.75 m, Fr = 7.9, Re = 59400, U_1 = 3.3 m/s, PD inflow conditions. Photo by Hubert Chanson.

Figure 13 corresponds to a Froude number of 5 whereas Figure 14 deals with a Froude number of 7.9. The free surface motion is more turbulent in the second case and flow aeration is much more important as well as found by Gualtieri and Chanson [28].

In the second part of this chapter, we aim to describe the most significant properties of the two-phase flow. Our interest is focused on void fraction, bubble count rate (bubble frequency), bubble velocity and mean bubble chord length. The present results are presented and compared with other experimental studies (mostly Gualtieri and Chanson [28], Kucukali and Chanson [31], Chanson [5, 12], Chanson and Brattberg [19] and Murzyn et al. [41, 42]).

2. Bubbly Flow Properties

The first basic property concerns the void fraction. Figure 15 presents three vertical dimensionless distribution of void fraction in hydraulic jumps with Froude numbers of 5.1, 7.6 and 8.3 with partially-developed inflow conditions. They correspond to the same relative distance downstream of the impingement point, $(x-x_1)/d_1$ = 12.5. Theoretical results are

plotted for the highest Froude number according to equation (5). Note that they are limited to the turbulent shear layer.

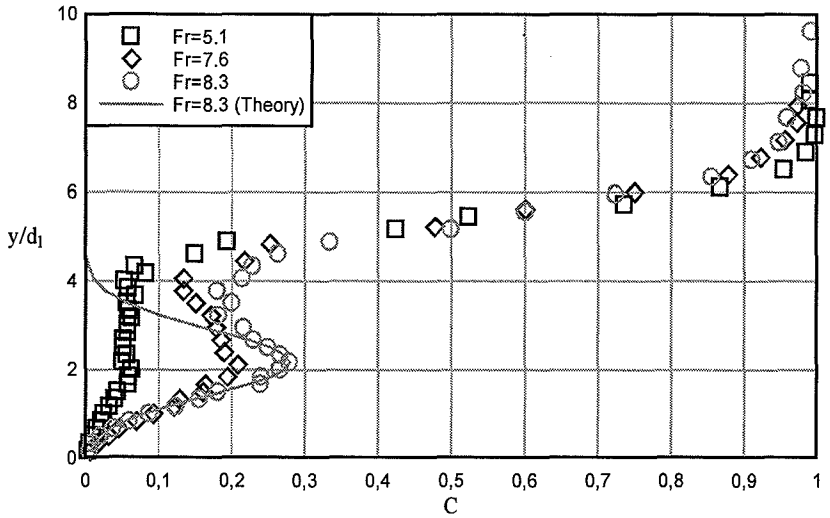

Figure 15. Dimensionless distribution of void fraction at $(x-x_1)/d_1$ = 12.5 for 3 different Froude numbers. Data from Murzyn and Chanson [38]. Comparison with theoretical solution of the diffusion equation (Eq. 5) $C = C_{max}\left(1 - \frac{\left(\frac{y - y_{C_{max}}}{d_1}\right)^2}{4D^*\left(\frac{x - x_1}{d_1}\right)}\right)$ for Fr = 8.3.

For all experimental conditions, this figure shows a rapid increase of the void fraction from the bottom up to a well-defined position called y_{Cmax}/d_1 where $C = C_{max}$. The corresponding peak of void fraction is clearly marked. Then, a slight decrease is observed. In the upper part of the flow (mixing layer or recirculation region), the void fraction increases again up to 100 % which corresponds to air. First, we note that theoretical solution of the diffusion equation is in agreement with the experimental data in the turbulent shear layer. At a given position $(x-x_1)/d_1$ downstream of the toe, it is evident that C_{max} changes with the Froude number. Whereas it is nearly 30% for Fr = 8.3, it is only 6.3% for Fr = 5.1. The highest values of C_{max} are found for the largest Froude numbers. This is confirmed by Figure 16 where C_{max} is plotted against $(x-x_1)/d_1$. At a fixed position downstream of the impingement point, it is obvious that the lower aeration correspond to the smallest Froude number. For a given Froude number, this Figure 16 also indicates that void fraction decreases when the distance to the toe increases.

Figure 17 describes the position of the maximum void fraction as a function of the distance to the toe. The vertical position y_{Cmax}/d_1 linearly increases with increasing the distance from the toe. Smaller shear stresses in the flow and larger buoyancy effects explain this trend. The best fit is given by equation (11):

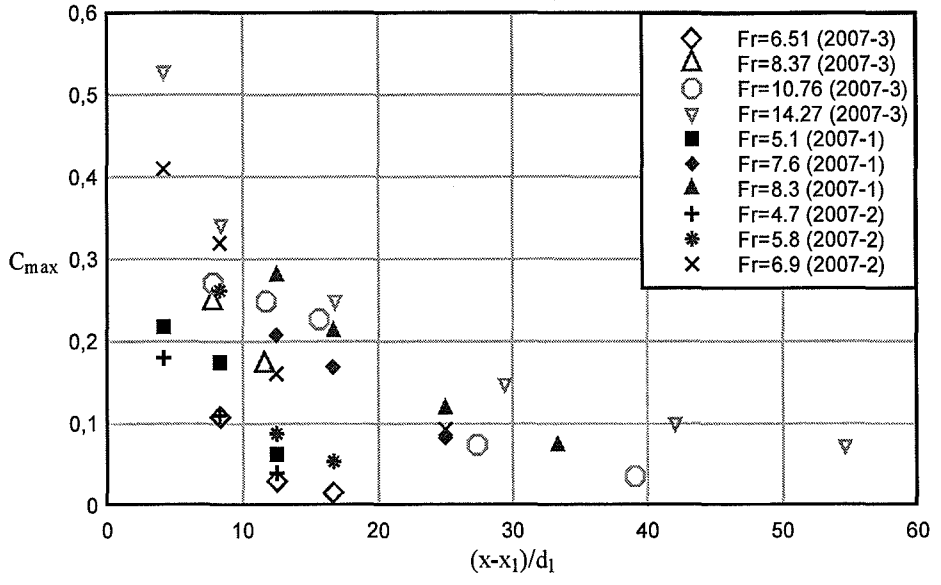

Figure 16. Dimensionless longitudinal distribution of maximum void fraction in the shear layer for different Froude numbers. 2007-1 refers to the experimental works of Murzyn and Chanson [38], 2007-2 to those of Kucukali and Chanson [31] and 2007-3 to those of Gualtieri and Chanson [28].

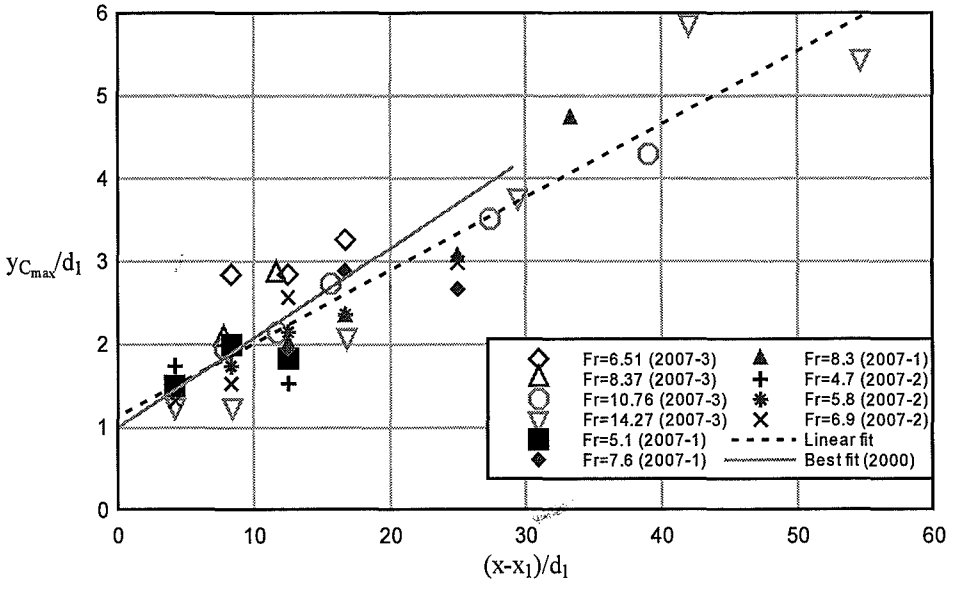

Figure 17. Dimensionless longitudinal distribution of y_{Cmax}/d_1 for different Froude numbers.2007-1 refers to the experimental works of Murzyn and Chanson [38], 2007-2 to those of Kucukali and Chanson [31], 2007-3 to those of Gualtieri and Chanson [28] and 2000 to those of Chanson and Brattberg [19].

$$\frac{y_{C_{max}}}{d_1} = 0.0881\frac{x - x_1}{d_1} + 1.134 \tag{11}$$

A comparison is also shown with the best linear fit obtained by Chanson and Brattberg [19]. For this study, measurements were performed with a smaller sensor. The close agreement between all data set would show that the main findings are nearly independent of the instrumentation characteristics.

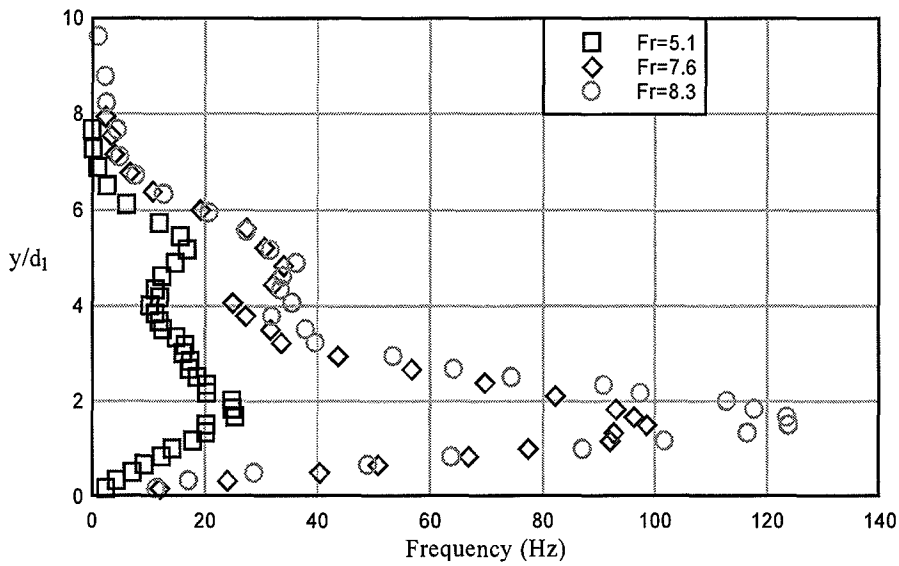

Figure 18. Vertical distribution of bubble count rate at $(x-x_1)/d_1 = 12.5$ for 3 different Froude numbers. Data from Murzyn and Chanson [38].

Figure 18 presents vertical distribution of bubble count rate at (x-x1)/d1 = 12.5 for different Froude numbers. It points out that the two distinctive peaks are measured. The first one (the most important) is found in the turbulent shear layer while the second one (minor peak) is at a higher elevation in the recirculating area. At a given position downstream of the toe, these maximum bubble count rates are related to the Froude number. F_{max} is only 25.4 Hz for Fr = 5.1 whereas it reaches 123.9 Hz for Fr = 8.3.

Dimensionless longitudinal distribution of y_{Fmax}/d_1 for different Froude numbers is shown on Figure 19. We observe the same linear trend as for y_{Cmax}/d_1. Nevertheless, the equation of the linear fit differs. Here, it is given by equation (12):

$$\frac{y_{F_{max}}}{d_1} = 0.073\frac{x - x_1}{d_1} + 0.6441 \qquad (12)$$

It indicates that the relative position of the maximum bubble count rate above the channel bottom increases with the distance to the toe. The data analysis of several data sets reveals that, for a given Froude number, the dimensionless maximum bubble count rate ($F_{max}d_1/U_1$) is a function of the distance to the toe (Figure 20). Furthermore, at a given distance $(x-x_1)/d_1$, $F_{max}d_1/U_1$ is also dependent on the Froude number. The highest bubble count rate is found for the largest Froude number.

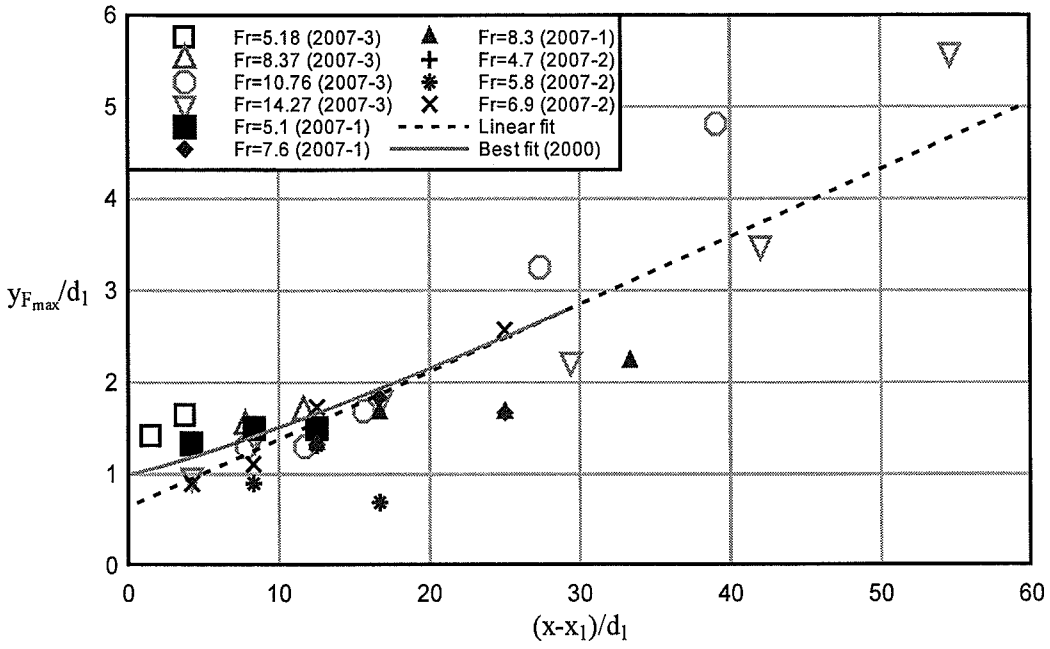

Figure 19. Dimensionless longitudinal distribution of y_{Fmax}/d_1 for different Froude numbers.

2007-1 refers to the experimental works of Murzyn and Chanson [38], 2007-2 to those of Kucukali and Chanson [31], 2007-3 to those of Gualtieri and Chanson [28] and 2000 to those of Chanson and Brattberg [19].

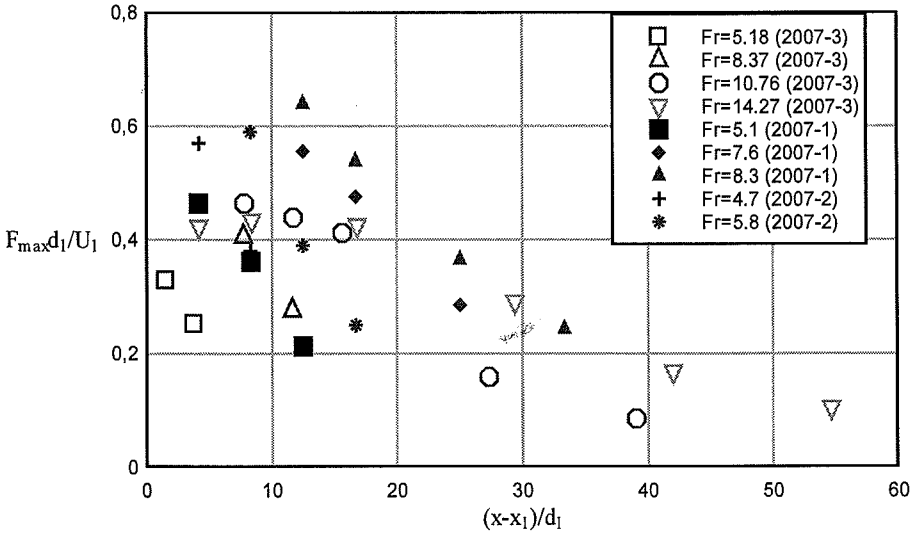

Figure 20. Longitudinal distribution of the dimensionless maximum bubble count rate $F_{max}d_1/U_1$ in the hydraulic jumps for different Froude numbers.2007-1 refers to experimental works of Murzyn and Chanson [38], 2007-2 to those of Kucukali and Chanson [31] and 2007-3 to those of Gualtieri and Chanson [28].

A close comparison of Figures 17 and 19 shows that the position of maximum bubble count rate is always below the maximum of air concentration whatever the Froude number is. Figure 21 clearly exhibits this trend.

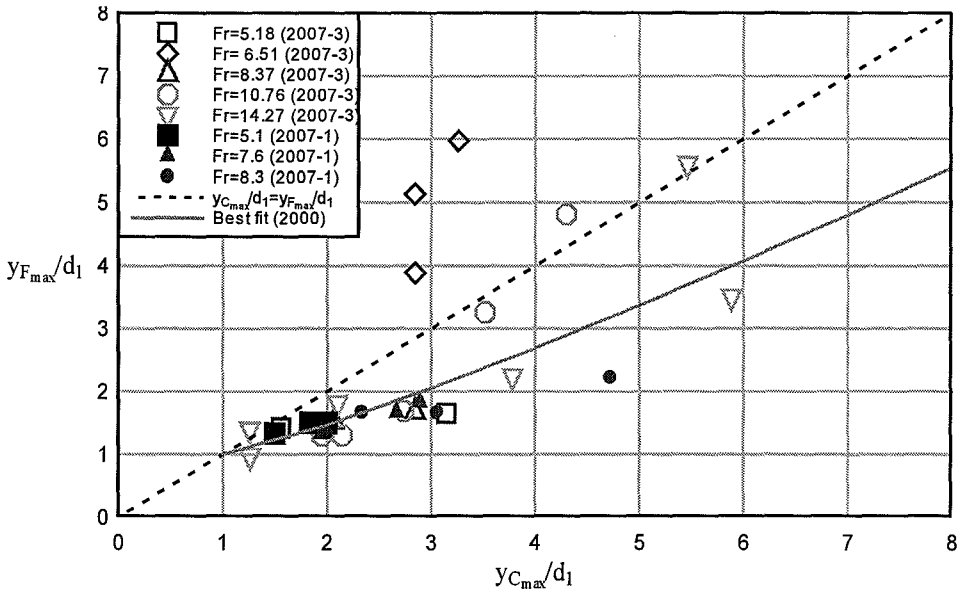

Figure 21. Dimensionless relationship between y_{Cmax}/d_1 and y_{Fmax}/d_1 in hydraulic jumps for different Froude numbers.2007-1 refers to the experimental works of Murzyn and Chanson [38], 2007-3 to those of Gualtieri and Chanson [28] and 2000 to those of Chanson and Brattberg [19].

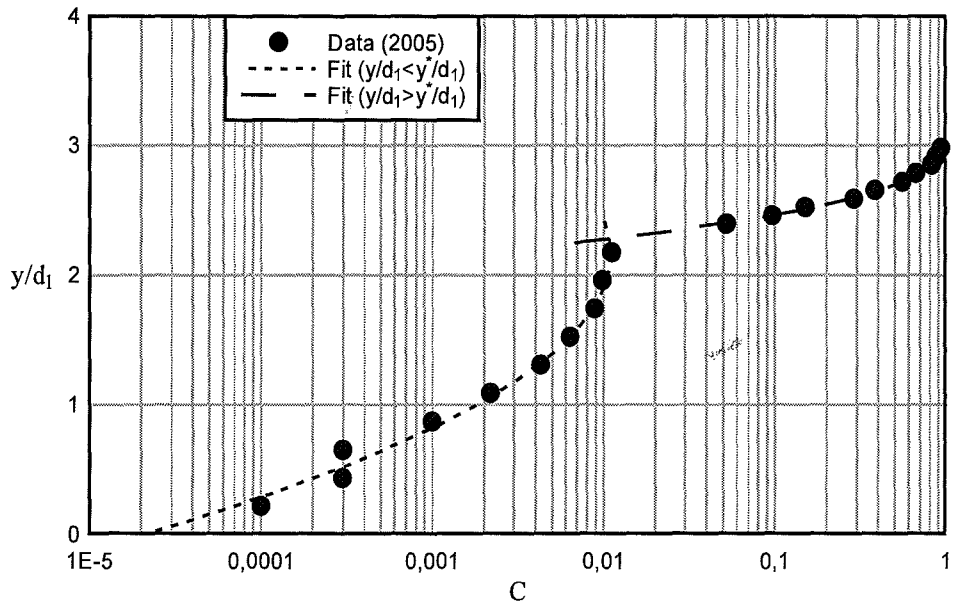

Figure 22. Typical void fraction distribution for Fr = 2.4 at $(x-x_1)/d_1$ = 8.7. The lower part of the data corresponds to the turbulent shear layer while the upper part is related to the mixing layer.Data 2005 refers to experimental works of Murzyn et al. [41].

This finding was first observed by Chanson and Brattberg [19]. In 2006, Chanson [12] argued that it could be due to a "*double diffusion process where vorticity and air bubbles diffuse at a different rate and in a different manner downstream of the impingement point*". This situation would mean some dissymmetric turbulent shear stress. Indeed, at a given void fraction, it is well-known the maximum bubble count rate is generally found in regions of high shear and large velocity.

The distinction between the turbulent shear layer and the recirculating region is obvious when plotting dimensionless void fraction vertical profile Figure 22 presents one classical flow condition obtained by Murzyn et al. [41]. A marked separation is observed at a given elevation y^*/d_1. In the lower part, C follows equation (5) whereas in the upper part it is best fitted by an error function [41]. Figure 23 shows the position y^*/d_1 for different experimental conditions investigated by Gualtieri and Chanson [28]. A comparison with data fit of Murzyn et al. [41] is plotted as well showing strong agreements between both studies.

Figure 24 describes dimensionless distributions of bubble velocity V/U_1 for different Froude numbers and for $(x-x_1)/d_1 < 15$. Data of Kucukali and Chanson [31] are plotted and compared with those of Murzyn and Chanson [38]. Considering the boundary condition on the channel bottom (no slip condition), these profiles point out the development of a boundary layer next to the bottom. This thin layer is characterized by a rapid increase of the velocity over a short distance. Then, a maximum is reached which is followed by a decay of the bubble velocity. Although some data scattering (due to the intrusive technique), the thickness of the boundary layer increases gradually with the distance to the toe. These data, compared to the experimental work of Rajaratnam [45] confirmed the similarity of the velocity profiles with those obtained for a wall-jet flow.

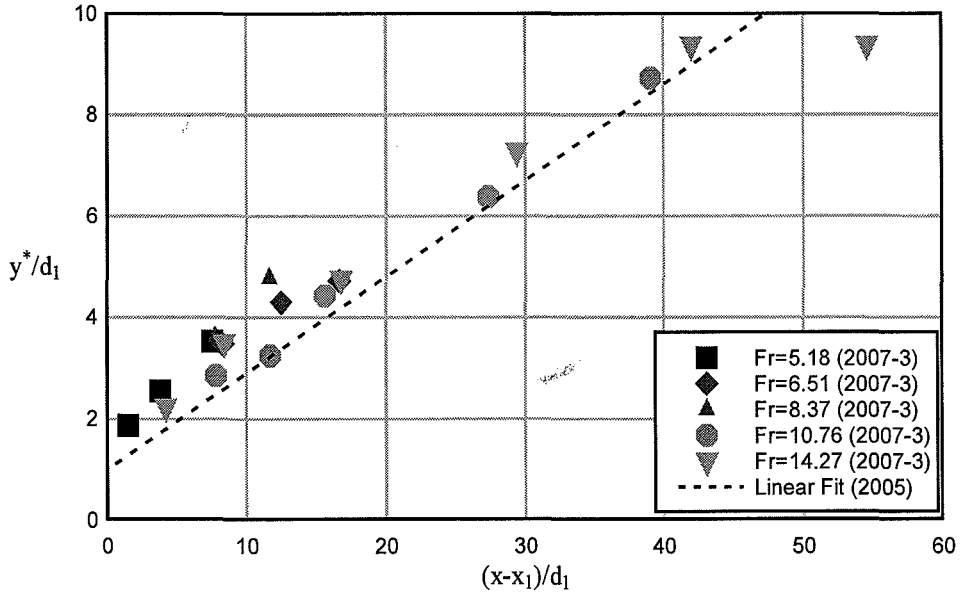

Figure 23. Dimensionless position of the boundary between the turbulent shear layer and mixing layer.2007-3 refers to experimental works of Gualtieri and Chanson [28] and 2005 to those of Murzyn et al. [41].

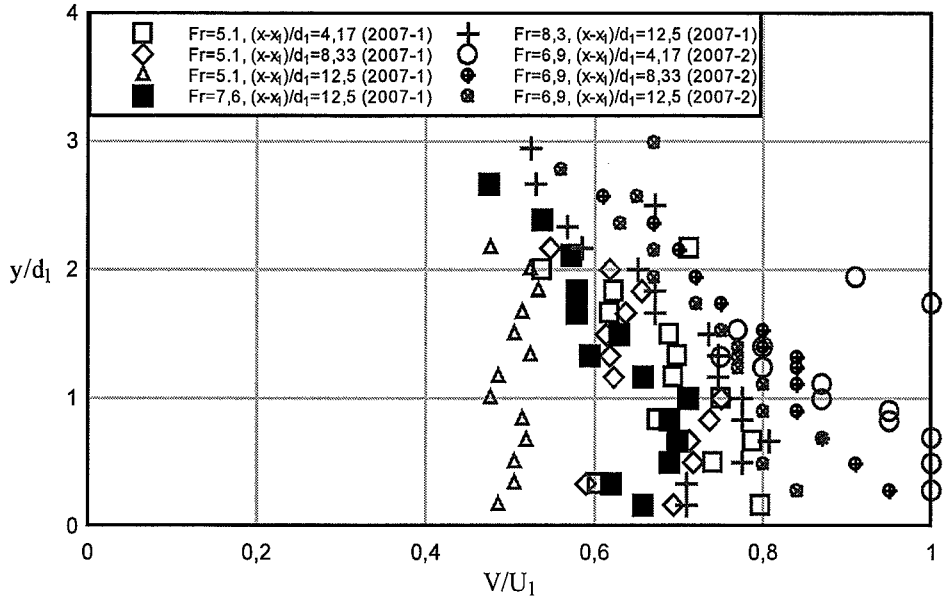

Figure 24. Dimensionless distributions of interfacial velocity V/U1 for $(x-x_1)/d_1 < 15$ for different Froude numbers.2007-1 refers to experimental works of Murzyn and Chanson [38] and 2007-2 to those of Kucukali and Chanson [31].

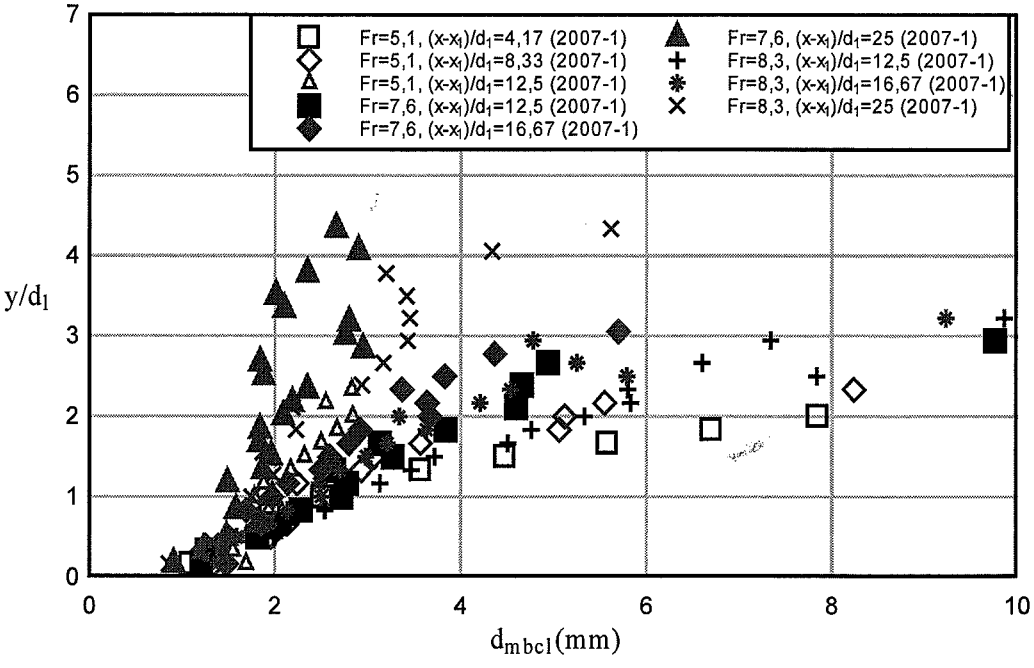

Figure 25. Distribution of mean bubble chord length in hydraulic jumps for different Froude numbers and $(x-x_1)/d_1 < 25$.2007-1 refers to experimental works of Murzyn and Chanson [38].

Figure 25 presents the mean bubble chord length for different Froude numbers and $(x-x_1)/d_1 < 25$. Data are those of Murzyn and Chanson [38]. The data indicate that maximum mean bubble chord length do not exceed 10 mm in the turbulent shear layer. This is in agreement with photos, visual observations and videos made during the experiments. Furthermore, the smallest bubbles are found to be closed to the bottom. At a given position $(x-x_1)/d_1$, the smallest bubbles were found in the region of higher shear stress. The order of magnitude is in agreement with those observed in previous studies [31, 41].

3. Free Surface, Sprays and Splashing

The free surface has been investigated using different experimental techniques. The most significant contributions regarding its dynamics with acoustic displacement meters are due to Kucukali and Chanson [31] and Murzyn and Chanson [38]. Other studies include Mouazé et al. [37] and Murzyn et al. [42] with wire gages and Chanson [6, 11, 12], Mossa and Tolve [36], Kucukali and Chanson [31] and Murzyn and Chanson [38] for flow visualizations. While acoustic displacement meters and flow visualizations are non invasive, wire gages are intrusive. Nevertheless, their size (wire diameter = 0.05 mm) ensures minimized disturbances. Photographic techniques and conductivity probes were also used to study the free surface [6, 31, 38]. In this part, we aim to present some results that bring information on the air/water interface. This is an important point because its large amplitude (spatial) motions and rapid (temporal) variations affect the mixing.

Figure 26 shows the harbour of Fécamp (Seine Maritime, France) during a storm in winter. On the right part of the bottom, the white color of the water demonstrates a large mixing of air and water due to the wave breaking associated with strong turbulence. This spilling breaking may be considered as a moving hydraulic jump. On the picture, other spilling breakers are seen showing important air/sea gas exchanges. While in-situ measurements are quite difficult in such weather conditions, experimental studies are more practical and needed to investigate the physical mechanisms involved in turbulent processes.

Figures 27 to 34 are flow visualizations made at the University of Southampton. The flume was 0.3 m in width. The Froude number ranges from 1.98 to 4.82 with 0.021 m < d_1 < 0.059 m with upstream velocity between 1.14 m/s and 2.19 m/s. On the left part, zooms on the toe are presented while on the right part, the entire width of the flow is seen.

During experiments on hydraulic jumps, oscillations of the front of the jump are often observed with frequency less than 1 hertz. At the University of Southampton, a 10 mm square bar was placed across the floor of the channel 1.2 m downstream of the foot. This improved the stability of the hydraulic jump. According to Mossa and Tolve [36], Chanson [12] and Murzyn and Chanson [38], based on the oscillation frequency of the toe, the Strouhal number is between 0.0038 and 0.013 for Froude numbers between 4.6 and 8.6.

Figure 26. Harbour of Fécamp (Seine Maritime, France) during a storm. Courtesy of Frédéric Malandain.

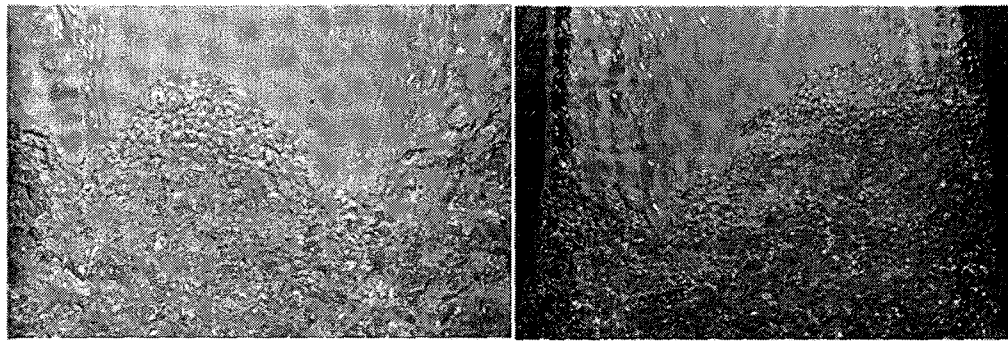

(27) (28)

Figures 27-28. Front toe of the hydraulic jump for Fr = 1.98. Flow from top to bottom. Left: zoom on the toe (27), Right: Front toe of the jump (28).Experimental conditions: Fr = 1.98, d_1 = 0.059 m, U_1 = 1.5 m/s On the left, the width corresponds to approximately 22 cm. On the right, the vertical walls of the flume can be seen: the horizontal image csize orresponds to about 30 cm.

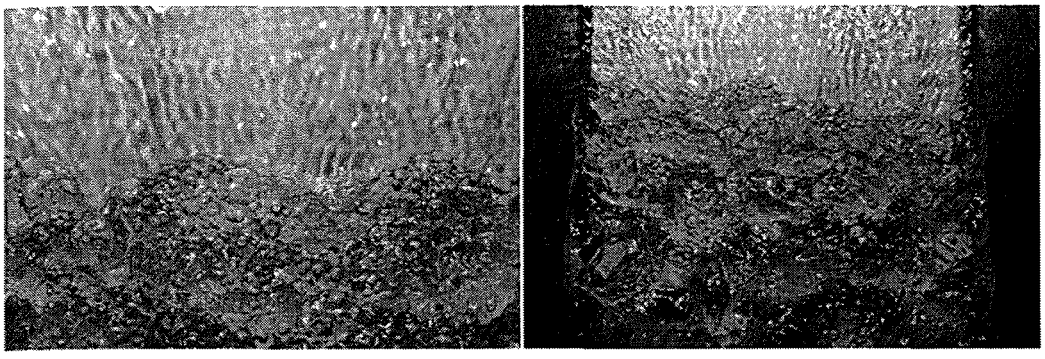

(29) (30)

Figures 29-30. Front toe of the hydraulic jump for Fr = 2.13. Flow from top to bottom. Left: zoom on the toe (29), Right: Front toe of the jump (30). Experimental conditions: Fr = 2.13, d_1 = 0.029 m, U_1 = 1.14 m/s On the left, the width corresponds to approximately 22 cm. On the right, the vertical walls of the flume can be seen: the horizontal image size corresponds to about 30 cm.

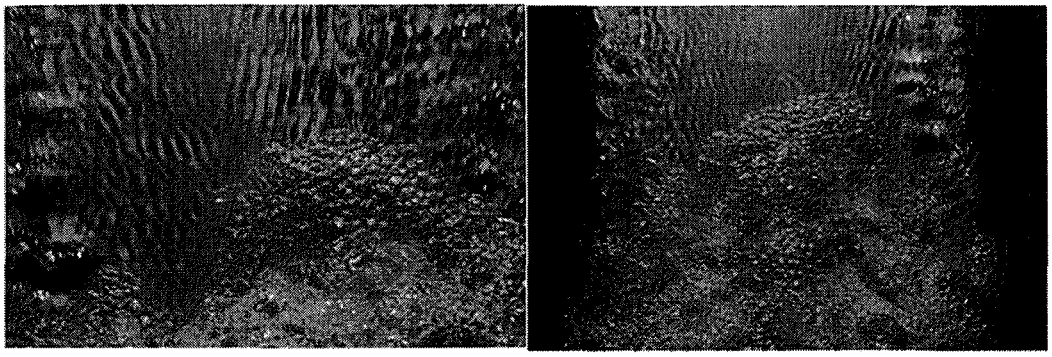

(31) (32)

Figures 31-32. Front toe of the hydraulic jump for Fr = 3.65. Flow from top to bottom. Left: zoom on the toe (31), Right: Front toe of the jump (32).Experimental conditions: Fr = 3.65, d_1 = 0.032 m, U_1 = 2.05 m/sOn the left, the width corresponds to approximately 22 cm. On the right, the vertical walls of the flume can be seen: the horizontal image size corresponds to about 30 cm.

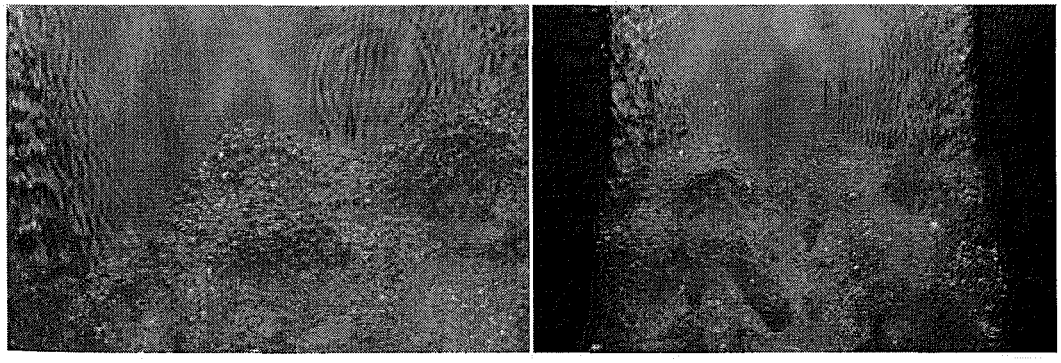

(33) (34)

Figures 33-34. Front toe of the hydraulic jump for Fr = 4.82. Flow from top to bottom. Left: zoom on the toe (33), Right: Front toe of the jump (34).Experimental conditions: Fr = 4.82, d_1 = 0.021 m, U_1 = 2.19 m/sOn the left, the width corresponds to approximately 22 cm. On the right, the vertical walls of the flume can be seen: the horizontal image size corresponds to about 30 cm.

From figures 27 to 34, Froude number increases. Much more bubbles are observed and the front of the toe becomes more and more turbulent. The aeration increases with Froude number and different length and time scales are measured depending on the inflow conditions. The gate aperture seems to be of primary importance regarding length scales developing at the free surface. Side views tend to confirm this (Figures 13 and 14).

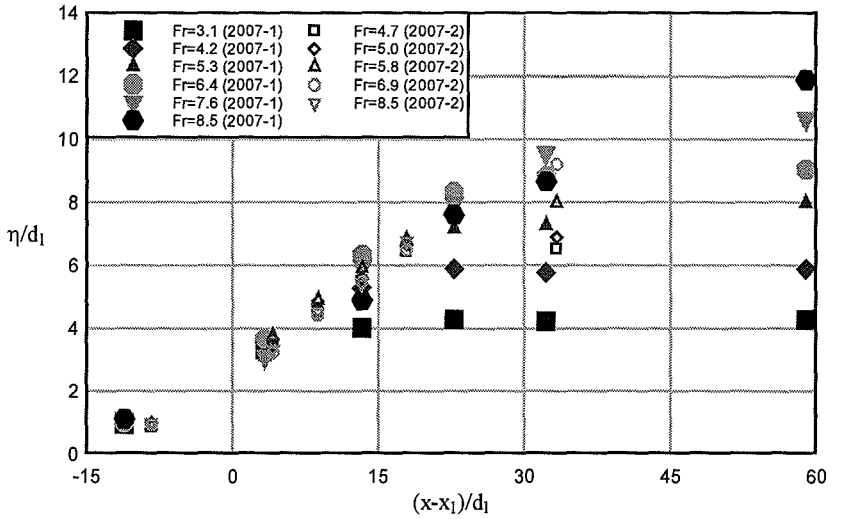

Figure 35. Dimensionless free surface levels in hydraulic jumps for different Froude numbers. 2007-1 refers to experimental works of Murzyn and Chanson [38] and 2007-2 to those of Kucukali and Chanson [31].

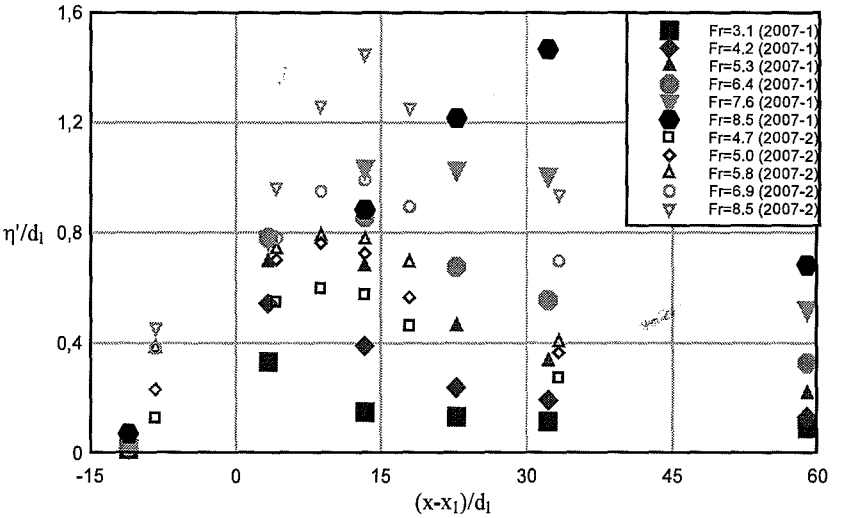

Figure 36. Dimensionless turbulent fluctuations of the free surface in hydraulic jumps for different Froude numbers. 2007-1 refers to experimental works of Murzyn and Chanson [38] and 2007-2 to those of Kucukali and Chanson [31].

Figure 35 presents the longitudinal dimensionless free surface profiles for Froude numbers up to 8.5. These experimental results correspond to measurements made at the University of Queensland at Brisbane by Kucukali and Chanson [31] and Murzyn and Chanson [38] using ultrasonic displacement meters. For $(x-x_1)/d_1 > 0$, a regular increase of the free surface is observed. Then, a constant level is reached (which corresponds to the dissipation area). For the highest Froude numbers, a constant level is not always observed. Indeed, only six acoustic displacement meters were used which was not sufficient enough. Nevertheless, the profiles (shapes) are in agreement with flow observations made during experiments and previous studies [31, 37, 42].

On Figure 36, the turbulent fluctuations of the free surface are plotted for the same experimental conditions. The same shapes are depicted for all Froude numbers. A rapid increase is noticed and a peak of turbulent fluctuations is reached in the first half of the roller. This corresponds to a turbulence production region. Then, a regular decrease is measured indicating a dissipative area.

The roller length can be deduced from the mean free surface levels. It corresponds to the length over which the free surface increases. Results are plotted on figure 37 and compared to previous studies made at the University of Southampton by Murzyn et al. [42] and presented by Chanson [10] showing strong agreements. The best linear fit is given showing that the roller length is proportional to the Froude number according to relation (13):

$$\frac{L_r}{d_1} = 6.26(Fr - 1.2) \tag{13}$$

This relation is obtained considering that air entrainment starts at Fr = 1.2. This hypothesis is meaningful regarding some laboratory experiments [15, 16, 42].

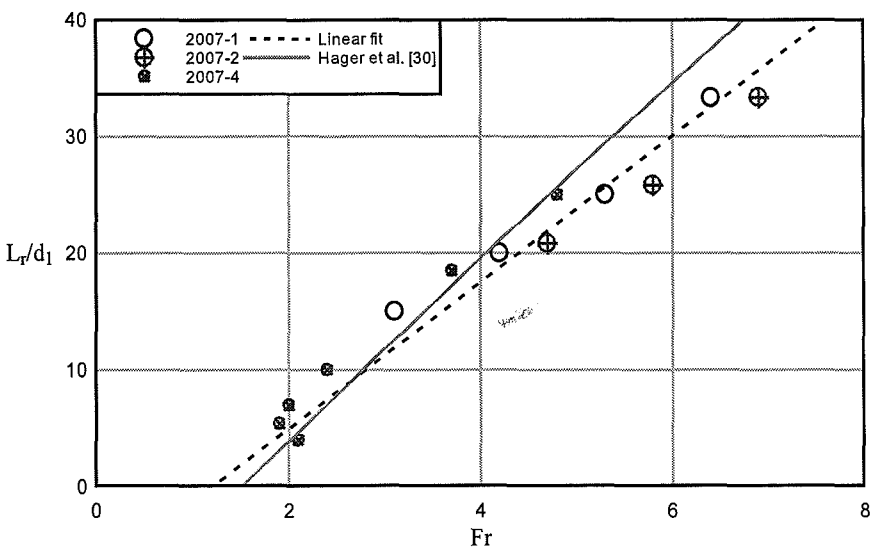

Figure 37. Dimensionless length of the roller in hydraulic jumps for different Froude number. 2007-1 refers to experimental works of Murzyn and Chanson [38], 2007-2 to those of Kucukali and Chanson [31], 2007-4 to those of Murzyn et al. [42] and Hager et al. [30] to the correlation of Hager and co-workers as presented by [10].

Based on a correlation technique, output signals of the wire gages can be analyzed to study the integral length and time scales of the structures developing at the free surface. Figure 38 presents the results regarding the dimensionless longitudinal length scales of turbulence for different Froude numbers. These results were obtained by Murzyn et al. [42] in the context of a research project which aimed to study the strong turbulence developing at the free surface. These length scales correspond to the size of the largest structures developing at the free surface. It is also a measure of the longitudinal length scale of vortical structures advecting air bubbles [12]. The figure shows that longitudinal turbulence length scale grows with the distance to the impingement point.

It ranges from less than $0.5d_1$ to $3d_1$. It also demonstrates that the upstream aperture has a strong influence on the turbulent structures developing in the jump. The best fit is given by:

$$\frac{L_f}{d_1} = 0.06\frac{x - x_1}{d_1} + 0.35 \tag{14}$$

Figure 39 describes the dimensionless transverse length scales of turbulence. They are related to the structures developing at the free surface perpendicular to the mean flow direction. They can be seen in Figure 30. The same trend is observed as for L_f/d_1. Transverse length scales of turbulence grow with the distance to the toe. They do not exceed more than $2d_1$ for most of the experimental conditions. They are smaller than L_f/d_1 and the best fit is given by:

$$\frac{L_g}{d_1} = 0.11\frac{x - x_1}{d_1} + 0.14 \tag{15}$$

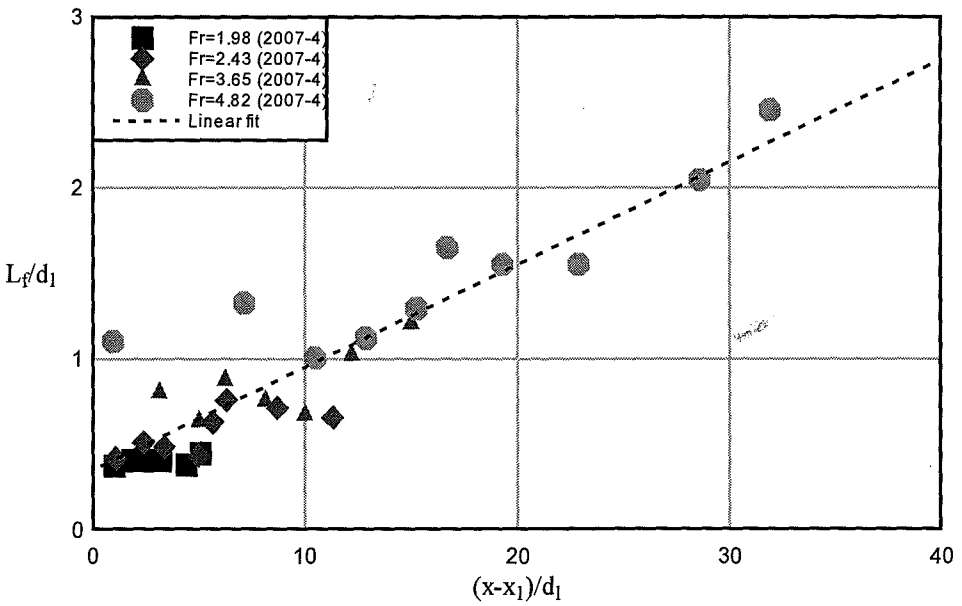

Figure 38. Dimensionless distributions of the streamwise turbulence length scales of the free surface measured by wire gages in hydraulic jumps for different Froude number. 2007-4 refers to experimental works of Murzyn et al. [42].

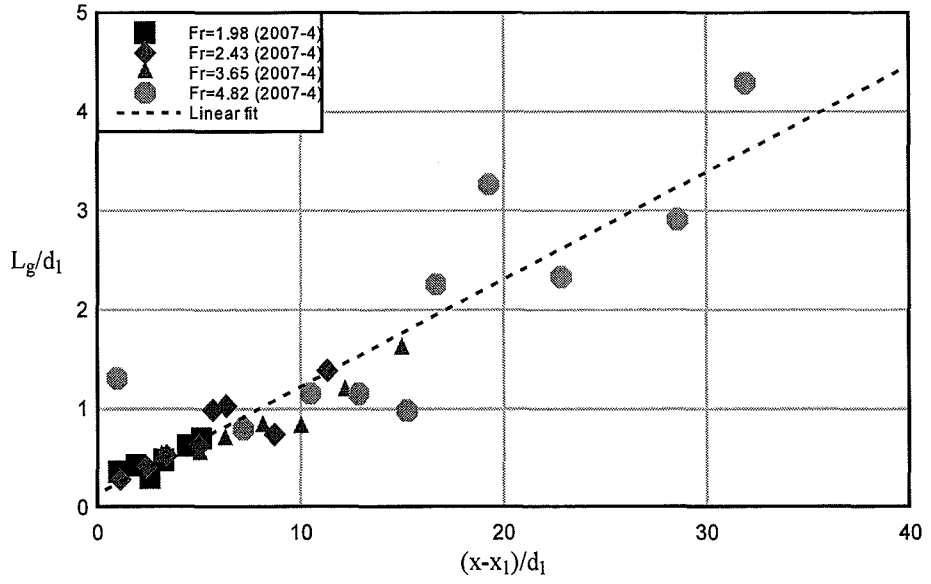

Figure 39. Dimensionless distributions of the transverse turbulence length scales of the free surface measured by wire gages in hydraulic jumps for different Froude number. 2007-4 refers to experimental works of Murzyn et al. [42].

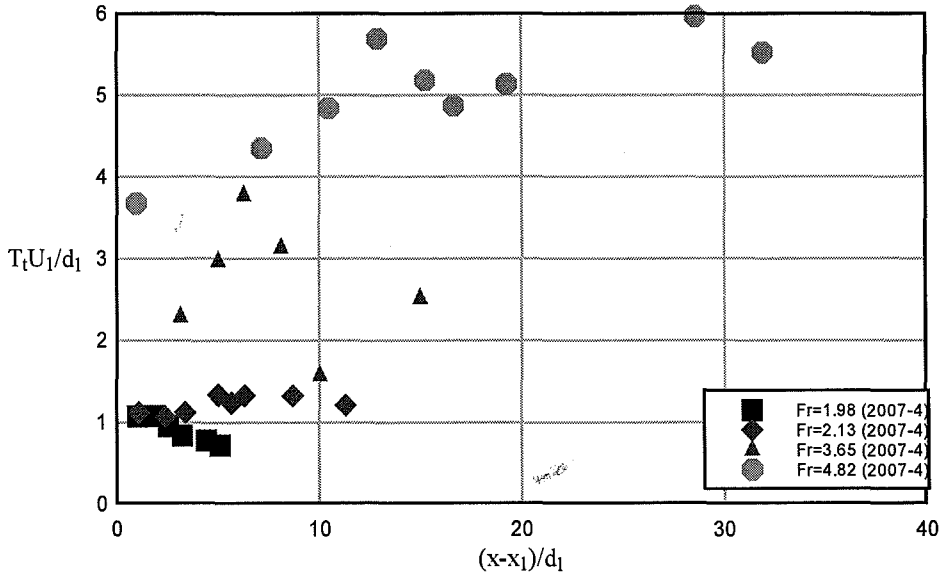

Figure 40. Dimensionless distributions of the turbulence time scales of the free surface measured by wire gages in hydraulic jumps for different Froude number. 2007-4 refers to experimental works of Murzyn et al. [42].

From auto-correlation measurements, integral time scales can be deduced. They represent the "lifetime" of the largest structures developing at the free surface. Figure 40 presents dimensionless integral time scales of turbulence as a function of the distance to the impingement point for different Froude numbers. Contrary to the longitudinal and transverse

length scales of turbulence, a dependence on the Froude number is depicted in Figure 40. The highest time scales are found for the highest Froude numbers. At a given position downstream of the toe, T_tU_1/d_1 increases with Fr. Lastly, T_tU_1/d_1 increases with the distance to the impingement point until a maximum is reached. Then, a slight decrease is observed.

4. Turbulence

Information on turbulence properties of the air-water flow can be obtained through optical or conductivity probes. With a dual-tip conductivity probe, correlation analysis can be undertaken to get details on the turbulent structure of the flow. The aim of this part is to present some results deriving from several experiments [12, 13, 23, 31, 38, 39, 40]. We are particularly interested in turbulence intensity and turbulence length and time scales.

The turbulence intensity is derived from a cross-correlation analysis between the two tips of the dual-tip conductivity probes. These were aligned either in the streamwise direction or perpendicular to the mean flow. Murzyn and Chanson [38] used dual-tip probes aligned in the streamwise direction and separated by a distance $\Delta x = 7$ mm. Data analysis was led on the output signals of the sensors to get some turbulence intensities and integral time scales. From a theoretical point of view, this approach is based on the relative width of the auto and cross correlation functions. The procedure was first presented and detailed by Chanson and Toombes [24, 25]. Further relevant references include Chanson [8, 12, 13], Chanson and Carosi [20, 21, 22] and Carosi and Chanson [4]. Thus, the turbulence intensity was deduced from the shapes of the cross-correlation R_{xz} and auto-correlation R_{xx} functions:

$$Tu = 0.851 \frac{\sqrt{\tau_{0.5}^{\ 2} - T_{0.5}^{\ 2}}}{T} \tag{16}$$

where $\tau_{0.5}$ is the time scale for which the normalized cross-correlation function is half of its maximum value such as $R_{xz}(T+\tau_{0.5}) = (R_{xz})_{max}/2$, $(R_{xz})_{max}$ is the maximum cross-correlation coefficient for $\tau=T$, $T_{0.5}$ is the time for which the normalized auto-correlation function equals 0.5 (Figure 41). More details can be found in Murzyn and Chanson [38].

The turbulence intensity characterizes the fluctuations of the interfacial velocity. Typical results are presented on Figure 42 for different experimental conditions. These results show very high levels of turbulence intensity up to 500 %. The most important levels are found close to the impingement point for the highest Froude numbers. For a given Froude number, the turbulence intensity decays with the distance to the toe. Furthermore, the turbulence intensity rapidly increases with the distance to the bottom. Far from the toe, the dimensionless distributions show a homogeneous distribution over the whole water depth.

An analysis of the auto-correlation function provides some information on the turbulent time scales (T_{xx}) of the flow. This treatment was applied to the leading tip in order to get T_{xx}. This integral time scale characterizes the streamwise coherence of the two-phase flow. This is also an estimation of the longest longitudinal connection in the air-water flow structure.

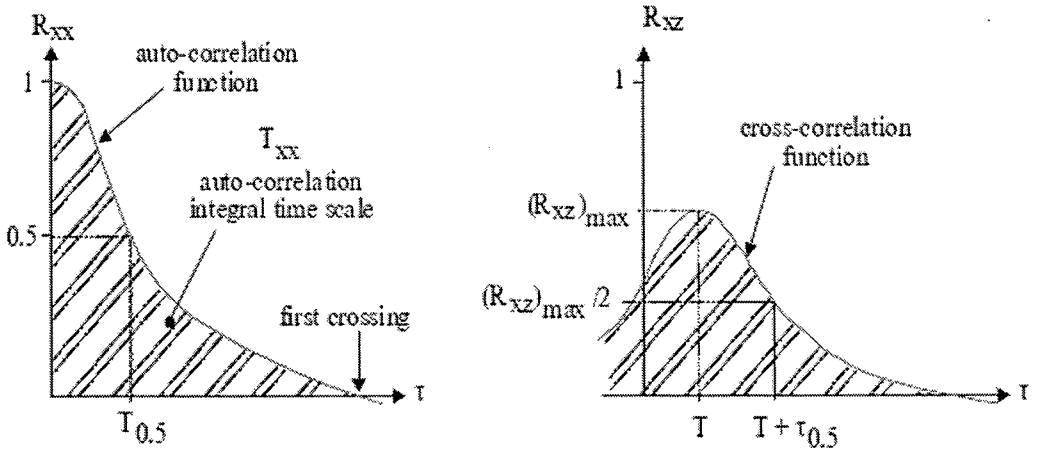

Figure 41. Definition sketch of the auto and cross-correlation functions for a dual-tip phase detection probe [12].

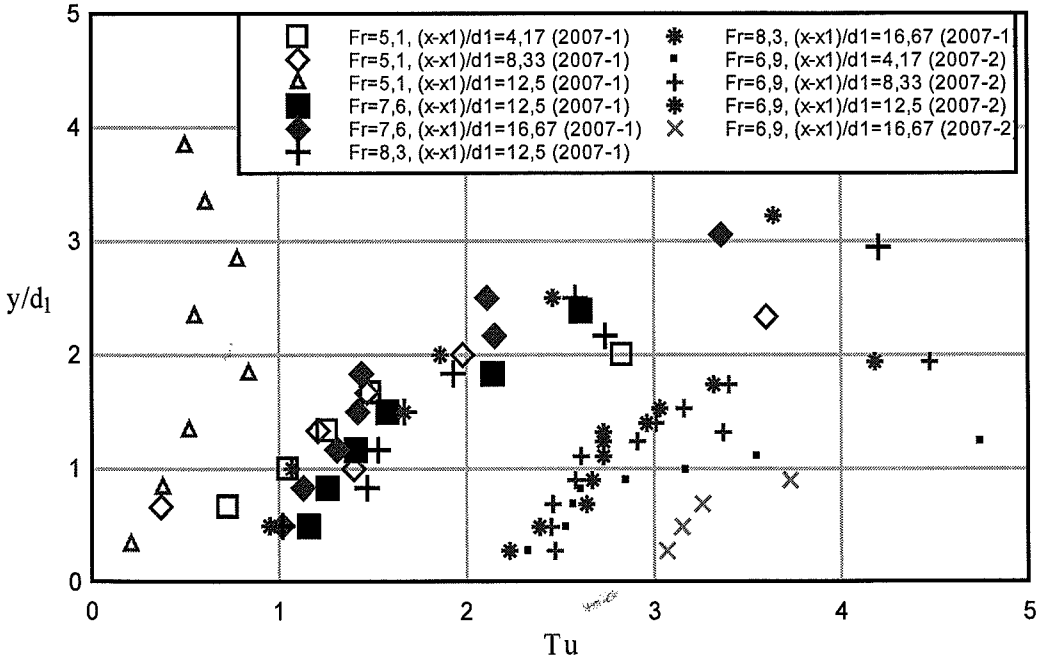

Figure 42. Dimensionless distributions of streamwise turbulence intensity Tu in hydraulic jumps for $(x-x_1)/d_1 < 20$. 2007-1 refers to experimental works of Murzyn and Chanson [38] and 2007-2 to those of Kucukali and Chanson [31].

Figure 43 presents results obtained for different experimental conditions corresponding to different Froude numbers.

Results show that integral time scales range from 0 (bottom of the channel) to less than 12 ms. Similar trends are found whatever the experimental conditions are. The integral time scales grow linearly from the bottom of the channel up to the free surface. This suggests that

the largest structures develop in the turbulent shear layer up to the air-water interface. Far downstream, the vertical profiles tend to be homogeneous with constant integral time scales.

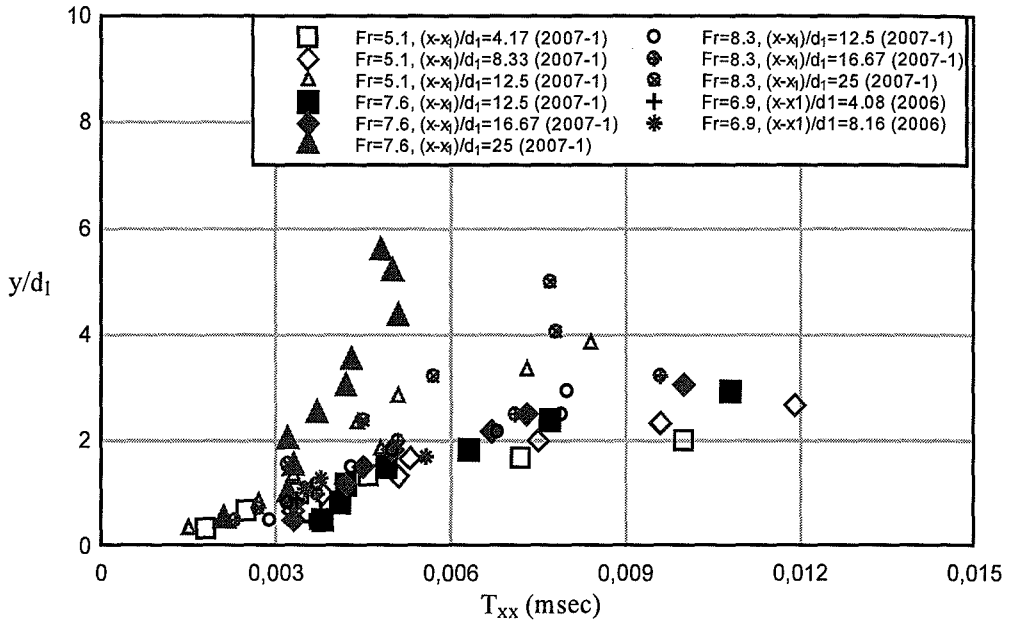

Figure 43. Distributions of auto-correlation integral time scales (Txx) in hydraulic jumps for $(x-x_1)/d_1 < 25$. 2007-1 refers to experimental works of Murzyn and Chanson [38] and 2006 to those of Chanson [12].

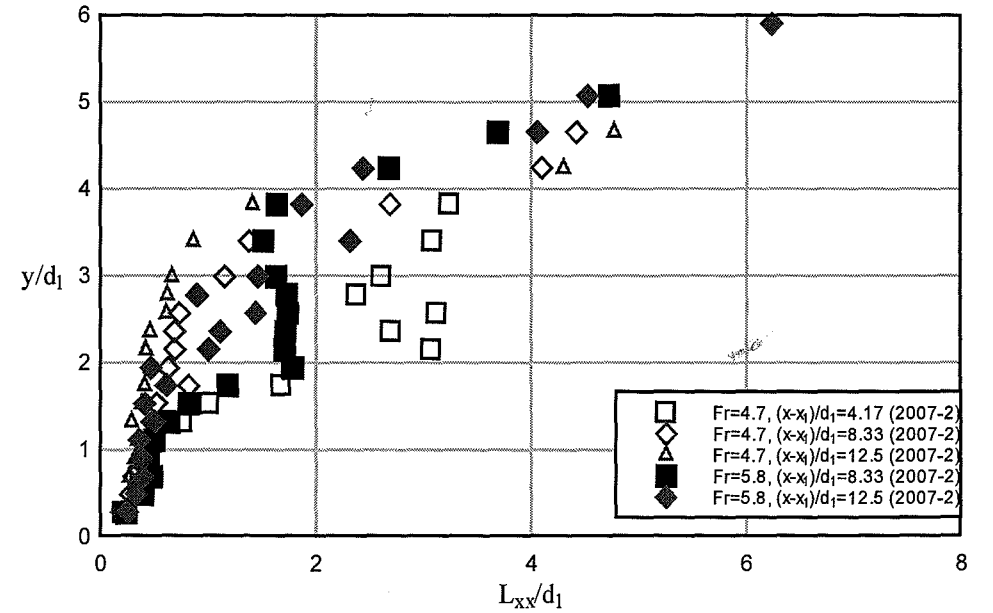

Figure 44. Dimensionless distributions of longitudinal integral length scales (Lxx/d1) in hydraulic jumps for $(x-x_1)/d_1 < 20$. 2007-2 refers to experimental works of Kucukali and Chanson [31].

Associated with integral time scales, integral length scales can also be defined. They provide information on the largest structures developing in the air-water flow. Chanson [12, 13] gave description of the behavior. Some results are presented on Figure 44 for the longitudinal integral length scales and on Figure 45 for the transverse integral length scale.

Their results indicate that both longitudinal and transverse integral length scales increase with relative flow depth. Whereas L_{xz}/d_1 ranges from 0 to 1, L_{xx}/d_1 grows from 0 to more than 6 showing a preferential stretching in the streamwise direction. The largest structures are also found close to the free surface. It is also evident that length scales become larger as the Froude number increases.

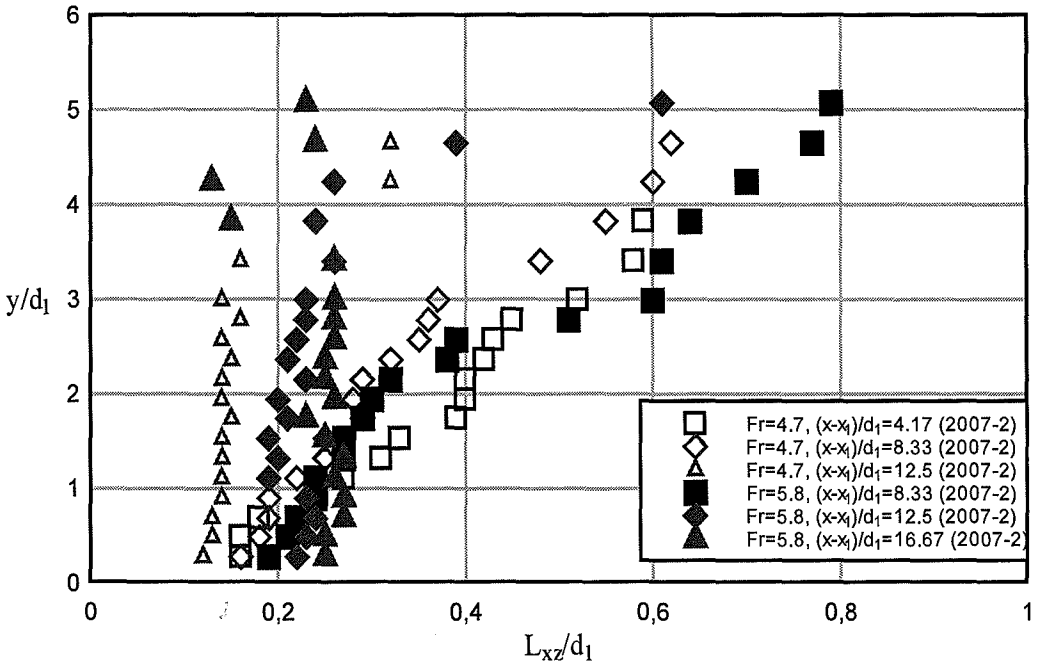

Figure 45. Dimensionless distributions of transverse air-water integral length scales (L_{xz}/d_1) in hydraulic jumps for $(x-x_1)/d_1 < 25$. 2007-2 refers to experimental works of Kucukali and Chanson [31].

All these results provide important information regarding the air-water flow properties and turbulence. They bring useful information on the structure of the hydraulic jump flow. They may be helpful for many reasons. For instance:

- They improve our knowledge on the flow dynamics by providing information on diffusion processes, bubble size, bubble frequency, void fraction…;
- They may provide interesting data to calibrate numerical codes. Indeed, the turbulence length and time scales give an idea for sizes and "lifetime" of the turbulent structure developing in the flow;
- They allow the development of new experimental techniques such as the optical probes used by Murzyn et al. [41] that were not used before in such flows. They allow new investigations in flows with length and time scales that are smaller and

faster than before. Furthermore, the sensor dimensions decrease increasing thus the accuracy of the results;
- They may contribute to improve and develop new methods for data analysis that could be used for other studies;
- They may give new insights on other problems such as spilling breaker on a beach, mixing and diffusion processes...

Nevertheless, there is still an important lack of knowledge on the field that requires further investigations. In the next part, we develop some examples of further research topics to study in the future.

5. Conclusions and Perspectives

The two-phase gas-liquid flow properties have been investigated by many researchers using different experimental techniques. Basic results were clearly found in terms of void fraction, bubble frequency and bubble velocity vertical profiles. A similitude with wall-jet flows was demonstrated. Some information on a double diffusion process were suggested as well. The turbulent flow structures were discussed in terms of both the free surface and the two-phase flow. Yet the huge amount of available data still needs further investigations and analyses. The present knowledge should be improved to assist the numericians to develop and calibrate their codes. Furthermore, new research topics may be developed with a focus on fundamental issues. Some developments have already started. The most promising research areas are probably those on bubble clustering, assessment of scale effects, effect of water quality on the flow properties and the influence of bubbles on sediment transport (three-phase flow).

In terms of bubble clustering, significant contributions were recently published for stepped cascades flows [25], dropshaft flows [9] and hydraulic jumps [12, 13]. By cluster, one means a groupment of two or more bubbles separated from other bubbles by a "significant distance". In the cluster, bubbles are close together and surrounded by a "sizeable volume of water". In the context of this chapter, the basic relevant references are [12, 13]. In these experimental works, two complementary approaches were presented [12, 13]. First, a clustering analysis is based upon the study of water chord time between adjacent bubbles. Second, a study is led on the interparticle arrival time. The main conclusions were obtained by analyzing the longitudinal flow structure [13]. These showed comparatively little bubble clustering in the air-water shear layer region. However, an interparticle arrival time analysis suggested some preferential bubble clustering for bubble chord times below 3 ms within the investigated flow conditions. Altogether both approaches are complementary but the interparticle arrival time analyses give a greater insight into the range of particle classes affected by non-random clustering. A further study was based on the analysis of the water chord time statistics [26, 27]. A cluster was recorded when a water chord time was less than 10 % of the median water chord time. The results showed that the number of bubbles associated with cluster in hydraulic jumps was around 21 % and this percentage decreases with increasing Froude number. They also showed that the average number of bubbles per cluster was 2.3 with mostly 2 bubbles per detected cluster: 70 % to 95 % of the clusters contain 2 bubbles [27]. These results may be helpful to assess vorticity production rate and bubble-turbulence interactions as well as new typical turbulent scales of the flow. Note that

these works are unfinished and further experiments are then required and new developments needed to assess these characteristics.

Recently, the effects of water quality on bubble entrainment and dispersion were investigated in circular plunging jet flows [17, 18]. This kind of flow has several applications including waste-water treatment or river re-oxygenation (Figure 46). Based upon laboratory experiments under controlled flow conditions using conductivity probes, the results demonstrated that lesser air entrainement takes place in seawater for identical experimental conditions compared to freshwater [17, 18]. Furthermore, they showed more fine bubbles in seawater than in freshwater or salty freshwater. Two main reasons may explain these findings. Living organisms may inhibite bubble entrainment. Furthermore, the surfactant and biochemicals are thought to harden the induction trumpet at plunge point, implying that surface tension σ could play a role in the air-water entrapment process. Nevertheless, its influence on the turbulent length scales developing at the free surface were investigated independently [42]. The results suggested that the longitudinal length scales of the free surface (L_f) do not depend upon the Weber number ($We = U_1\sqrt{\frac{\rho d_1}{\sigma}}$) but mostly by the upstream water depth d_1.

Figure 46. Strong mixing of air and water at Vallée de la Gatineau, Québec, Canada. Le Grand Remous viewed from le Pont Couvert Savoyard, July 2002. Photo by Hubert Chanson.

Scale effects may be very significant. Although it is easier to undertake laboratory experiments instead of in-situ measurements, one must be sure that results obtained from

these experiments would be also true in nature. A study assessed the scale effects affecting two-phase flow properties in hydraulic jumps [39]. Based upon hydraulic jumps with identical Froude number (Fr = 5 and 8.5) but with different Reynolds numbers ranging from 24000 to 98000, the results demonstrated some drastic scale effects in the smaller hydraulic jumps in terms of void fractions, bubble count rate and bubble size. Simply dynamic similarity can not be achieved with a Froude similitude only and viscous effects may be significant even with Reynolds numbers larger than 10^5 as illustrated in [23, 39].

One challenging research topic deals with the interaction between air, water and solid particles. This is particularly encountered in coastal environments where sediments are entrapped by wave breaking or in river engineering during flood periods (Figure 47). Figure 47 illustrates a hydraulic jump in a muddy creek. The brownish colour of the waters is evidences of the large sediment suspension load. To date, these three-phase flows are too complex to be fully understood, with too many equations and parameters to be taken into account. For numerical modeling, fully non linear equations strongly increase the difficulties [3] and available experimental data are very limited. Even with the most powerful computers, it is not conceivable that the flow dynamics could be fully understood in the close future. Furthermore, exact similitude can not be achieved because of the numerous paramaters such as sediment size, density, shapes, flow scales... In situ measurements are also difficult because of the invasive technique used which disturb the flow and the dangers associated with the field measurements in a river in flood (Figure 47). Drastic progresses are needed in this field to ensure a better comprehension of the phenomena.

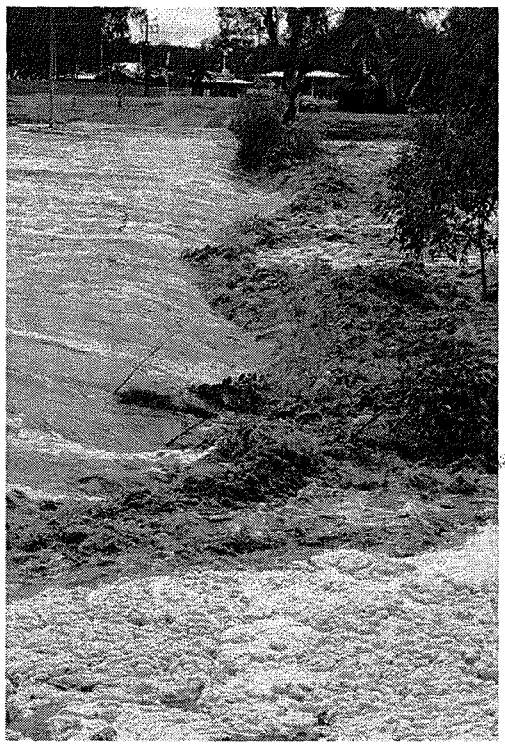

Figure 47. Todd river in Alice Springs NT (Australia), January 2007. A complex mixing of water, air and sediment during floods (1 in 5 or 1 in 10 years flood). Courtesy of Sue McMINN.

Acknowledgements

The first author thanks François Stephan, head of department at ESTACA Paris (Ecole Supérieure des Techniques Aéronautiques et de la Construction Automobile, http://www.estaca.fr) for his support and Frédéric Malandain (Cany-Barville, France, http://www.frederic-malandain.fr/) for providing nice pictures of Normandy's coastlines.

References

[1] Babb A.F., Aus H.C. Measurements of air in flowing water, *Journal of Hydraulic Division, ASCE*, **107** (HY12), 1981, pp 1615-1630.

[2] Bélanger J.B. *Essai sur la solution numérique de quelques problèmes relatifs au mouvement permanent des eaux courantes*, Carialian-Goeury, Paris, France, 1828 (in french).

[3] Brennen C.E. *Fundamentals of multiphase flows*, Cambridge University Press, 2005, 345 pages.

[4] Carosi G. Chanson H. Air-water time and length scales in skimming flows on a stepped spillway. Application to the spray characterization, Research Report CH59/06, Department of Civil Engineering, The University of Queensland, Brisbane, Australia, July 2006, 142 pages.

[5] Chanson H. Air entrainment in two dimensional turbulent shear flows with partially-developed inflow conditions, *International Journal of Multiphase Flow*, **31**, 6, 1995, pp 1107-1121.

[6] Chanson H. *Air bubble entrainment in free surface turbulent shear flows*, Academic Press, London, UK, 1997, 401 pages.

[7] Chanson H. *The hydraulics of open-channel flow : an introduction*, Edward Arnold, London, UK, 1999, 512 pages.

[8] Chanson H. Air-water flow measurements with intrusive phase-detection probes. Can we improve their interpretation? *Journal of Hydraulic Engineering, ASCE*, **128**, 3, 2002, pp 252-255.

[9] Chanson H. An experimental study of Roman dropshaft operation : hydraulics, two-phase flow, acoustics, Report CH 50/02, Department of Civil Engineering, The University of Queensland, Brisbane, Australia, 2002, 99 pages.

[10] Chanson H. The hydraulic of open-channel flow : an introduction, Butterworth-Heinemann, Oxford, UK, 2nd edition, 2004, 630 pages.

[11] Chanson H. Bubble entrainment, spray and splashing at hydraulic jumps, *Journal of Zhejiang University Science A*, **7**, 8, 2006, pp 1396-1405.

[12] Chanson H. Air bubble entrainment in hydraulic jumps. Similitude and scale effects, Research Report CH57/05, Department of Civil Engineering, The University of Queensland, Brisbane, Australia, January, 2006, 119 pages.

[13] Chanson H. Bubbly flow structure in hydraulic jump, *European Journal of Mechanics*, **26**, 3, 2007, pp 367-384.

[14] Chanson H. Dynamic similarity and scale effects affecting air bublle entrainment in hydraulic jumps, *Proceedings of the 6th International Conference on Multiphase Flow*

ICMF 2007, Leipzig, Germany, July 9-13, M. Sommerfeld Editor, Session 7, 2007, 11 pages.

[15] Chanson H. Hydraulic jumps: bubbles and bores, 16th Australasian Fluid Mechanics Conference AFMC, Crown Plaza, Gold Coast, Australia, December 2-7, P. Jacobs, T McIntyre, M. Cleary, D. Buttsworth, D. Mee, R. Clemens, R. Morgan, C. Lemcker Editors, 2007, Plenary Address, pp 39-53.

[16] Chanson H. Current knowledge in hydraulic jumps and related phenomena. A survey of experimental results, *European Journal of Mechanics* B/Fluids, in press, 2008.

[17] Chanson H., Aoki S.I., Hoque A. Scaling bubble entrainment and dispersion in vertical circular plunging jet flows : freshwater versus seawater, *Proceedings of the 5th International Conference on Hydrodynamics*, Tainan, Taïwan, 2002.

[18] Chanson H., Aoki S.I., Hoque A. Bubble entrainment and dispersion in plunging jet flows : freshwater versus seawater, *Journal of Coastal Research*, **22**, 3, 2006, pp 664-677.

[19] Chanson H., Brattberg T. Experimental study of the air-water shear flow in a hydraulic jump, *International Journal of Multiphase Flow*, **26**, 4, 2000, pp 583-607.

[20] Chanson H., Carosi G. Advanced post-processing and correlation analyses in high-velocity air-water flows. 1- Macroscopic properties, *Proceedings of the International Junior Researcher and Engineer Workshop on hydraulic structures (IJREWHS'06)*, Montemor-o-Novo, Jorge Matos and Hubert Chanson Eds, Report CH61/06, Division of Civil Egineering, The University of Queensland, Brisbane, Australia, December 2006, pp 139-148.

[21] Chanson H., Carosi G. Advanced post-processing and correlation analyses in high-velocity air-water flows. 1- Microscopic properties, *Proceedings of the International Junior Researcher and Engineer Workshop on hydraulic structures (IJREWHS'06)*, Montemor-o-Novo, Jorge Matos and Hubert Chanson Eds, Report CH61/06, Division of Civil Egineering, The University of Queensland, Brisbane, Australia, December 2006, pp 149-158.

[22] Chanson H., Carosi G. Turbulent time and length scale measurements in high-velocity open-channel flows. *Experiments in Fluids*, **42**, 3, 2007, pp 385-401.

[23] Chanson H., Gualtieri C. Similitude and scale effects of air entrainment in hydraulic jumps, *Journal of Hydraulic Research*, **46**, 1, 2008, pp 35-44.

[24] Chanson H., Toombes L. Experimental investigations of air entrainment in transition and skimming flows down a stepped chute. *Application to embankment overflow stepped spillways*, Research Report CE158, Department of Civil Engineering, The University of Queensland, Brisbane, Australia, July, 2001, 74 pages.

[25] Chanson H., Toombes L. Air-water flows down stepped chutes: turbulence and flow structure observations, *International Journal of Multiphase Flow*, **28**, 11, 2002, pp 1737-1761.

[26] Gualtieri C., Chanson H. Clustering process and interfaccial area analysis in a large-size dropshaft, *Advances in Fluid Mechanics* V, A. Mendes, M. Rahman, C.A. Brebbia Editors, WIT Press, 2004.

[27] Gualtieri C., Chanson H. Clustering process analysis in a large-size dropshaft and in a hydraulic jump, *32nd IAHR Biennial Congress*, Venice, July 2007, 11 pages.

[28] Gualtieri C., Chanson H. Experimental analysis of Froude number effect on air entrainment in the hydraulic jump, *Environmental Fluid Mechanics*, **7**, 2007, pp 217-238.

[29] Hager W.H. Energy dissipators and hydraulic jump, Kluwer Academic Publisher, *Water Science and Technology Library*, Volume 8, Dordrecht, The Netherlands, 288 pages.

[30] Hager W.H., Bremen R., Kawagoshi N. Classical hydraulic jump: length of roller, *Journal of Hydraulic Research, IAHR*, **28**, 5, 1990, pp 591-608.

[31] Kucukali S., Chanson H. *Turbulence in hydraulic jumps: experimental measurements, Report CH62/07*, Department of Civil Engineering, The University of Queensland, Brisbane, Australia, July 2007, 96 pages.

[32] Lennon J.M., Hill D.F. Particle Image Velocity measurements of undular and hydraulic jumps, *Journal of Hydraulic Engineering*, **132**, 12, 2006, pp 1283-1294.

[33] Liu M., Zhu D.Z., Rajaratnam N. Evaluation of ADV measurements in bubbly two-phase flows, Proceedings of the conference on Hydraulic Measurements and Experimental Methods, EWRI, Tony L. Wahl, Clifford A. Pugh, Kevin A. Oberg, Tracy B. Vermeyen (Editors), Estes Park, USA, 2002.

[34] Matos J., Frizell K.H., André S., Frizell K.W. On the performance of velocity measurement techniques in air-water flows, Proceedings of speciality conference "Hyraulic Measurements and Experimental Methods", *EWRI, ASCE, IAHR*, Estes Park, USA, August 2002, 11 pages.

[35] Mossa M. On the oscillating characteristics of hydraulic jumps, *Journal of Hydraulic Research, IAHR*, **37**, 4, 1999, pp 541-558.

[36] Mossa M. Tolve U. Flow visualization in bubbly two-phase hydraulic jump, *Journal of Fluids Engineering,* **120**, 1998, pp 160-165.

[37] Mouazé D., Murzyn F., Chaplin J.R. Free surface length scale estimation in hydraulic jumps, *Journal of Fluids Engineering, Transaction of ASME*, **127**, 2005, pp 1191-1193.

[38] Murzyn F., Chanson H. Free surface, bubbly flow and turbulence measurements in hydraulic jumps, Report CH63/07, *Division of Civil Engineering*, The University of Queensland, Brisbane, Australia, July, 2007, 113 pages.

[39] Murzyn F., Chanson H. Experimental assessment of scale effects affecting two-phase flow properties in hydraulic jumps, *Experiments in Fluids*, in press *(corrected proofs)*, 2008, 9 pages.

[40] Murzyn F., Chanson H. Experimental investigation of bubbly flow and turbulence in hydraulic jumps, Environmental Fluid Mechanics, in press (*corrected proofs*), 2008, 17 pages.

[41] Murzyn F., Mouazé D., Chaplin J.R. Optical fibre probe measurements of bubbly flow in hydraulic jumps, *International Journal of Multiphase Flow*, **31**, 1, 2005, pp 141-154.

[42] Murzyn F., Mouazé D., Chaplin J.R. Air-water interface dynamic and free surface features in hydraulic jumps, *Journal of Hydraulic Research* **45**, 5, 2007, pp 679-685.

[43] Prosperetti A., Tryggvason G. Computational methods for multiphase flow, Cambridge University Press, 2007, 470 pages.

[44] Rajaratnam N. An experimental study of air entrainment characteristics of the hydraulic jump, *Journal of Instrumental Engineering,* The Institution of Enginners (India), 42, 7, 1962, pp 247-273.

[45] Rajaratnam N. The hydraulic jump as a wall jet, *Journal of Hydraulics Division*, HY 5, 1965, pp 107-132 (+ Discussion HY 3, pp 110-123, + Closure HY 1, pp 74-76).

[46] Resch F.J., Leutheusser H.J. Le ressaut hydraulique : mesure de turbulence dans la région diphasique, *La Houille Blanche*, **4**, 1972a, pp 279-293.

[47] Resch F.J. Leutheusser H.J. Reynolds stress measurements in hydraulic jumps, *Journal of Hydraulic Research*, **10**, 4, 1972b, pp 409-429.

[48] Waniewski T.A., Hunter C., Brennen C.E. Bubble measurements downstream of hydraulic jumps, *International Journal of Multiphase Flow*, **27**, 2001, pp 1271-1284.

Reviewed by Dominique Mouazé
Lecturer
Morphodynamique Continentale et Côtière
University of Caen - Basse Normandie, 24 rue des Tilleuls, 14000 Caen (France)
E-mail address: dominique.mouaze@meca.unicaen.fr
Ph: +33.(0)2.31.56.57.11

MULTIPHASE FLOW RESEARCH

S. MARTIN
AND
J.R. WILLIAMS
EDITORS

Nova Science Publishers, Inc.
New York